Integrated solvent and process design using a SAFT-VR thermodynamic description: high-pressure separation of carbon dioxide and methane

F. E. Pereira, E. Keskes, A. Galindo, G. Jackson and C. S. Adjiman *

Centre for Process Systems Engineering,

Department of Chemical Engineering,

Imperial College London,

London SW7 2AZ, UK.

June 22, 2010

*Author to whom all correspondence should be addressed: Tel. +44 (0)20 7594 6638. Email: c.adjiman@imperial.ac.uk

Abstract

The increasing importance of natural gas as an energy source poses separation challenges, due to the high pressures and carbon dioxide concentrations of many natural gas streams. A methodology for computer-aided molecular and process design (CAMPD) applicable to such extreme conditions is presented, based on the integration of process and cost models with an advanced molecular-based equation of state, the statistical associating fluid theory for potentials of variable range (SAFT-VR). The approach is applied to carbon dioxide capture from methane using physical absorption. The search for an optimal solvent is focused on *n*-alkane blends. A simple flowsheet is optimised using two objectives: maximum purity and maximum net present value. The best equipment sizes, operating conditions, and average chain length of the solvent (the *n*-alkane) are identified, indicating *n*-alkane solvents offer a promising alternative. The proposed methodology can readily be extended to wider classes of solvents and to other challenging processes.

Keywords: solvent and process design; CAMD; CAMPD; SAFT; CO_2 capture; natural gas

1 Introduction

The removal of carbon dioxide (CO_2) from natural gas streams is an important industrial issue in the context of diminishing energy resources and CO_2 mitigation. Natural gas is usually produced at high pressure (for example, around 10MPa) and in extreme cases may have a CO_2 concentration of up to 70 mol %. This CO_2 reduces the calorific value of the natural gas, and the mole fraction of CO_2 must be reduced to below 3% before the gas may be introduced into distribution pipelines (Anderson & Siahaan, 2005). Natural gas streams also have very high flowrates, in the region of 100-1000 million standard cubic feet per day (MMSCFD), which means they can give rise to 70-700 MMSCFD of CO_2. This is comparable with the CO_2 emissions of a typical power station. As

the implementation of the Kyoto protocol requires the capture of large quantities of CO_2, the injection of CO_2 into depleted, or near-depleted, reservoirs for enhanced oil/gas recovery operations will become increasingly frequent. This is likely to result in gas streams that are even richer in CO_2, and that have an increasing CO_2 concentration over the lifetime of the gas field. The high flowrates, the wide ranges of pressures and compositions involved, and the variability of the natural gas composition make the optimal design of CO_2 removal processes an important and challenging topic.

General methodologies for the design of separation processes have been proposed based on heuristics and optimisation approaches for the identification of the flowsheet topology, equipment type (e.g., absorber, membrane modules), size, operating conditions, and control system that lead to the best process performance as quantified by criteria such as profitability and environmental impact (e.g., Pistikopoulos & Stefanis (1998); Hostrup, Harper & Gani (1999)). Many separation processes also necessitate the identification of suitable separating agents (e.g., solvents, membranes). Often, the choice of solvent is made prior to the design of the flowsheet structure and operating conditions. However, these decisions are closely linked, and the best process performance can only be achieved by considering them simultaneously as a computer-aided molecular and process design (CAMPD) problem. Several methods for formulating and solving such problems have been proposed. Pistikopoulos & Stefanis (1998) and Buxton, Livingston & Pistikopoulos (1999) have developed a multi-step multi-objective methodology based on a mixed-integer nonlinear programming (MINLP) formulation, in which a pre-processing step is added before the solution of the primal problem. This allows the quick evaluation of the separating agent put forward by the master problem, before the solution of the primal problem. This work has been applied to absorption processes and extended to dynamic models (Giovanoglou, Barlatier, Adjiman, Pistikopoulos & Cordiner, 2003). Another approach has been developed by Marcoulaki & Kokossis (2000), who have used a simulated annealing approach to integrate solvent and process design. Hostrup, Harper & Gani (1999) have proposed a hybrid method that

combines heuristics and mathematical programming to develop an optimal flowsheet and an optimal solvent. Eden, Jørgensen, Gani & El-Halwagi (2004) have proposed the removal of the constitutive equations from the process model, so that property targets are identified during process optimisation, independently of molecular structure. Molecules that can match the resulting property targets are then identified in a separate computer-aided molecular design (CAMD) problem. In this context, an alternative algorithm for the solution of the CAMD problem has recently been presented (Chemmangattuvalappil, Eljack, Solvason & Eden, 2009). Papadopoulos & Linke (2006, 2008) decompose the problem into a multi-objective property-based solvent design problem and a process design problem, with the integration of the two subproblems effected via clustering techniques. Finally, Bardow, Steur & Gross (2010) have recently proposed a two-stage methodology for integrated process and solvent design, termed continuous molecular targeting approach to CAMD (coMT-CAMD). In this work, parameters for an optimal solvent are found as part of a process optimisation problem, and these are mapped onto a real molecule via discrete decisions. A common feature of most approaches is that they are based on thermodynamic models that are typically reliable only at low pressures. Exceptions to this are the work of Cismondi, Diaz, Espinosa & Brignole (2003), in which the ECOFAC method is used together with the group contribution associating (GCA) equation of state (EOS) (Gros, Bottini & Brignole, 1997) to consider near-critical solvents and the methodology of Bardow, Steur & Gross (2010), which has been developed for the PCP-SAFT equation of state (Gross, 2005) and applied to CO_2 capture from a flue gas at low pressure.

In our work, we seek to demonstrate how advanced thermodynamic methods can be integrated into computer-aided process design so that the design of the solvent and the process for high-pressure separation can be tackled in an integrated manner.

The modelling of vapour-liquid equilibria (VLE) is an important source of uncertainties for the design of an absorption separation process. Dohrn & Pfohl (2002) discuss the impact of errors in the prediction of separation factors on

the minimum number of stages as predicted by the Fenske-Underwood equation. For example, for a separation factor of 1.2, a deviation of +/-5% in the separation factor leads to an error of between -20% and +40% on the required number of stages. An accurate representation of the VLE is particularly important in processes where the range of pressures and temperatures involved is large, such as in CO_2 separation from natural gas. If the absorption occurs at high pressure and the solvent regeneration is atmospheric, this can correspond to temperatures ranging from ambient to 450-500 K for some of the gas streams. The UNIFAC (universal functional activity coefficient) group contribution method (Fredenslund, Jones & Prausnitz, 1975) to model the liquid phase(s) and the assumption of ideality to represent the gas phase are typically used in CAMPD problems or for property-based solvent design (Odele & Macchietto, 1993; Gani & Brignole, 1983). The UNIFAC framework is attractive due to its simplicity, its high predictive accuracy for many complex systems, and the large number of groups for which parameters are available. One of its main limitations in the context of separation system design is that it is based on a lattice model of the fluid and cannot therefore cannot be used to capture the effect of pressure on the thermodynamic properties. Moreover, the assumption of ideality in the gas phase is a crude approximation for many systems even under low compression. There are thus many industrially important applications, such as the high-pressure absorption of CO_2 from natural gas, that cannot be tackled reliably with such techniques.

In this work, we develop a thermodynamic framework which can be used in CAMPD problems involving complex fluids over wide ranges of temperatures and pressures. It is based on using the statistical associating fluid theory for potentials of variable range (SAFT-VR) (Gil-Villegas, Galindo, Whitehead, Mills, Jackson *et al.*, 1997; Galindo, Davies, Gil-Villegas & Jackson, 1998) to represent the liquid and gas phases simultaneously, using a continuous representation to capture changes in the number of phases in the units. The SAFT-VR equation of state is well suited to design problems requiring the optimisation of molecular structure because it is rooted in a microscopic representation of the

fluid. As a result, it has been shown that SAFT-VR parameters can be readily transferred between molecules in a homologous series (McCabe, Galindo, Gil-Villegas & Jackson, 1998b; McCabe & Jackson, 1999; McCabe, Galindo, Gil-Villegas & Jackson, 1998a; Blas & Galindo, 2002; Galindo & Blas, 2002; Filipe, de Azevedo, Martins, Soares, Calado *et al.*, 2000; Filipe, Martins, Calado, McCabe & Jackson, 2000; Paricaud, Galindo & Jackson, 2004; McCabe, Galindo, Garcia-Lisbona & Jackson, 2001).

SAFT-based approaches are well suited to treating highly non-ideal asymmetric and associating systems and can be used to provide an accurate representation of both the liquid and gas phases, giving them an unusually wide range of applicability (Müller & Gubbins, 2001; Paricaud, Galindo & Jackson, 2002; Tan, Adidharma & Radosz, 2008). The use of an equation of state such as SAFT ensures that a single model can be used for all fluid phases. This has the advantage that all thermodynamic properties can be derived in a consistent framework, without requiring additional data. For instance, when UNIFAC is used, the heat capacities that are needed for energy balances are typically derived from a separate group contribution approach where ideal mixing is assumed. In contrast, in our proposed approach, heat capacities or enthalpies can be obtained from SAFT-VR without the need for an additional predictive model and without resorting to the assumption of ideal mixing. Furthermore, group contribution versions of SAFT-VR have recently been proposed (Tamouza, Passarello, Tobaly & de Hemptinne, 2004, 2005; Lymperiadis, Adjiman, Galindo & Jackson, 2007; Lymperiadis, Adjiman, Jackson & Galindo, 2008; Peng, Goff, dos Ramos & McCabe, 2009). The SAFT-γ version (Lymperiadis, Adjiman, Galindo & Jackson, 2007; Lymperiadis, Adjiman, Jackson & Galindo, 2008), which corresponds to a molecular model of heteronuclear chains of fused segments, based on SAFT-VR, has shown to be very promising in terms of predictive capability. As the group parameter table is expanded, this equation of state can be incorporated into the methodology proposed here. Alternative group contribution equations of state are also available, such as the predictive Soave-Redlich-Kwong (PSRK) EOS (Holderbaum & Gmehling, 1991; Li, Fischer & Gmehling, 1998)

or the volume-translated Peng-Robinson (VTPR) EOS (Ahlers & Gmehling, 2001, 2002a), although to our knowledge they have not yet been integrated in CAMPD methodologies.

The design of a process for CO_2 removal from natural gas is a challenging problem for CAMPD, and it is used in our current paper to assess the adequacy of the proposed approach. In Section 2, we identify a possible flowsheet and the basic design parameters for a new process for CO_2 removal from natural gas based on a physical absorption process, and present a generic CAMPD problem formulation. In Section 3, we present the transferable thermodynamic model at the heart of the approach. In Section 4, we develop a process model capable of handling changes in the number of phases in each unit, including a detailed economic assessment. Finally, in Section 5, we define the optimisation variables and constraints for a CO_2-capture process design and report the findings of our optimisation, using the natural gas inlet conditions from an Indonesian gas field (Anderson & Siahaan, 2005).

2 Methodology

The computer-aided solvent and separation process design problem can be stated as follows:

Given a feed mixture to be separated, determine the design (equipment sizes, operating conditions and solvent or solvent mixture) that gives the best performance.

The methodology followed in this work is based on two steps: (i) the identification of the design space (e.g., separation technique(s) to be considered, types of solvents to be used); and (ii) the formulation and solution of an optimisation problem that captures this problem statement within a single mathematical formulation.

In order to develop an appropriate mathematical representation, several process-specific modelling components are required. First, a thermodynamic

model that can describe the mixtures of interest must be developed. Since we use the statistical associating fluid theory for potentials of variable range (SAFT-VR), we must ensure that SAFT-VR molecular parameters are available to model the relevant mixtures.

The second modelling component is a steady-state process model based on a proposed flowsheet structure. One of the difficulties in developing a process model for integrated solvent and process design is that the simultaneous variation of the solvent and the operating conditions during the course of the optimisation can lead to unfeasible operation. For instance, one may find that a single phase is stable in a flash unit or that two phases exist within a compressor. This problem is more likely to occur when a process operates over a wide range of temperatures and pressures, as is the case in the application considered in this paper. The model equations must therefore include an appropriate test that can detect these phase changes.

The final modelling component is the economic evaluation of the process. For this purpose, standard correlations for the equipment sizes, in terms of operating conditions, are used (Ulrich, 1984; Douglas, 1988; Perry, Green & Maloney, 1997; Peters, Timmerhaus & West, 2002). The capital costs are estimated from the sizes. The operating costs are calculated based on the prices of material and energy and standard relations for other costs (e.g., labour, overheads). This allows one to calculate the net present value (NPV) of the process for a given plant life and interest rate, which may be used as the objective function. The optimisation problem may also be based on alternative objective functions, such as the effectiveness of the separation.

2.1 Identification of the design space

The specific problem of CO_2 removal from a high pressure natural gas stream is considered in order to identify a promising flowsheet and appropriate constraints.

2.1.1 Selection of separation technique

Techniques commonly used in the gas separation industry include adsorption onto solid substrates, chemical absorption, gas permeation, and physical absorption (Kohl & Nielsen, 1997). Adsorption is economical for comparatively small-scale purification, typically reducing the CO_2 content from 3% down to 0.5%, while chemical absorption has been used successfully for low-pressure gas streams containing between 3% and 25% of CO_2. Chemical absorption processes have very high selectivities, typically greater than 99%, but involve large solvent regeneration costs, which hamper their application to higher CO_2 contents. The absorption is limited by the stoichiometry of the chemical reaction (with an amine-to-CO_2 ratio of 2:1 for monoethanolamine) so that the use of this process for CO_2-rich gas streams will lead to high solvent circulation flowrates, large units and high energy requirements. Gas permeation techniques involve compact and flexible units, and can be easily adapted to changes in CO_2 content. However, reliability is a concern, especially because natural gas contaminants can lead to the deterioration of the membrane, and the selectivity is not typically as high as in the case of chemical absorption.

Physical absorption can also be used successfully. Its main advantage is the potentially greater absorption limits of physical absorption solvents with respect to CO_2. At high CO_2 partial pressure, the CO_2 loading capacity of the solvent has the potential to be high for a physical solvent. Hence, physical absorption processes are particularly appropriate for the treatment of high pressure CO_2-rich natural gas streams. The commercial viability of physical absorption processes for CO_2 capture with *n*-alkane solvents has already been exemplified by the successful application of the Ryan-Holmes cryogenic separation process (Holmes, Ryan, Price & Styring, 1982) to natural gas treatment.

The choice of solvent is one of the key decision variables impacting on the performance and economics of a physical absorption process. Many solvents have been used for the absorption of CO_2 and CH_4, including various formulations of tributyl phosphate, polycarbonate, methylcyanoacetate, and N-formyl

morpholine (Newman, 1985). Unfortunately, there are major drawbacks with all of these for practical operations; the solvents are not easily disposable and may be involved in side reactions with other natural gas constituents. A more suitable solvent, which is relatively inert and can easily be handled in an oil and gas environment, is n-butane; this is used in the aforementioned Ryan-Holmes process (Holmes, Ryan, Price & Styring, 1982). The Ryan-Holmes process has a satisfactory CO_2/CH_4 separation factor, but operation at low temperatures is very energetically demanding. Like n-butane, other alkanes, such as n-decane, are known to absorb CO_2 preferentially to CH_4 (Dunyushkin, Skripka & Nenartovich, 1977; Orr & Silva, 1983; Orr, Johns & Dindoruk, 1993; Blunt, Fayers & Orr, 1993), and the use of higher molecular-weight (longer) n-alkanes, or alkane blends, may provide a promising route towards adapting the Ryan-Holmes process to the temperatures and pressures typical of natural gas streams.

Based on the success of n-butane as a solvent in the Ryan-Holmes process, longer n-alkanes with correspondingly higher boiling points are investigated here in order to develop a non-cryogenic process. The identification of the optimal solvent requires one to establish an accurate description of the thermodynamic properties for the range of $n-$alkanes considered. We consider a range of solvents which possess suitable volatility and viscosity, between $n-$heptane (C_7) and $n-$tetradecane (C_{14}). The longer n-alkanes are likely to be too viscous while shorter n-alkanes are likely to be too volatile for the temperature range of interest. Branched alkanes would also be suitable candidate solvents, but we focus on the linear alkanes as it is easier to develop transferable molecular models in this case. Solvent mixtures may also be advantageous compared to pure compounds. For instance, consider a mixture of $n-$heptane (C_7) and $n-$eicosane (C_{20}): the longer alkane (C_{20}) would enhance the absorption of CO_2, while the presence of the shorter hydrocarbon (C_7) would ensure that the solvent remains liquid throughout the process and is not too viscous. The most desirable balance of these competing factors would be an optimal blend of n-alkanes of varying length, i.e., the solution to a solvent design problem.

2.1.2 A basic flowsheet for physical absorption

The proposed process strips the natural gas stream of CO_2 through physical absorption into an *n*-alkane solvent. A simple flowsheet is selected for the development of the methodology. More complex flowsheets, which yield better performance, are considered in detail in separate work (Pereira, Keskes, Galindo, Jackson & Adjiman, 2010). The basic flowsheet is shown in figure 1, and contains the following unit operations: one absorption column, one flash drum, two expansion valves, one mixer (mixing junction) and one pump.

The process operates as follows: The natural gas stream is expanded, to ensure a constant flowrate, and to allow control of the pressure in the absorber. It then enters the bottom of absorption column, where it comes into contact with an *n*-alkane solvent. The solvent absorbs CO_2 preferentially to CH_4 (Dunyushkin, Skripka & Nenartovich, 1977) so that the gaseous stream is consequently stripped of CO_2 as it makes its way towards the top of the column. The CO_2-enriched solvent leaving the bottom of the column is then expanded into a flash drum to form a CO_2-rich vapour phase and CO_2-lean liquid phase, which consists mostly of solvent. This regenerated solvent is recycled to a mixer where fresh solvent is added where necessary before the stream enters the top of the absorption column. The CO_2-rich vapour phase from the flash drum leaves the process for disposal, or further use. The cleaned gas stream, or sale gas, leaving the top of the absorber is sent for storage and retail. For simplicity, in this work we assume that the natural gas stream contains only CH_4 and CO_2.

The performance of the process depends on many factors. These include the thermodynamic properties of the solvent + CH_4 + CO_2 mixture, which are highly dependent on the process conditions. The extent of the absorption of CO_2 into a given solvent can be controlled by adjusting the temperature and pressure in the absorber. In addition, equipment sizing will affect both the degree of separation and also the process efficiency. In particular, the number of absorption/desorption stages plays an important role in the purity of the two outlet streams.

2.2 Generic CAMPD problem formulation

The generic CAMPD problem for a continuous steady-state process can be formulated as an optimisation problem as follows:

$$\begin{aligned} \max_{\boldsymbol{x},\boldsymbol{y}} \quad & f(\boldsymbol{x},\boldsymbol{y}) \\ \text{s.t.} \quad & h(\boldsymbol{x},\boldsymbol{y}) = 0 \\ & g(\boldsymbol{x},\boldsymbol{y}) \leq 0 \\ & \boldsymbol{x} \in \mathbb{R}^m \\ & \boldsymbol{y} \in \{0,1\}^q, \end{aligned} \tag{1}$$

where $\boldsymbol{x}$ is an m-dimensional vector of continuous variables denoting operating conditions, physical properties, process variables, solvent mixture composition, and equipment sizes; $\boldsymbol{y}$ is a q-dimensional vector of binary variables describing the structure of the solvent molecules; f is the objective function, which is typically an economic performance metric; h and g are sets of equality and inequality constraints, respectively. They include: structure-property constraints, which relate solvent molecular structure to physical properties; chemical feasibility constraints, which ensure that only chemically meaningful solvent molecules are designed; chemical complexity constraints, which limit the size of the molecule and the types of groups or combinations of groups that can be used in designing the molecule; equality constraints defining the process model, including mass and energy balances, and the thermodynamic model; inequality constraints on process performance, equipment sizing, and solvent performance, which may include constraints on environmental performance or on solvent physical properties such as toxicity or boiling point; an economic model, which relate process variables and equipment sizes to cost or revenue.

This generic formulation is typically a mixed-integer nonlinear programming problem (MINLP) due to the presence of binary variables to describe the molecular structure of the solvent(s). However, since the solvent design space for CO_2 removal from natural gas has been narrowed down to mixtures of n-alkanes, it will be shown in Section 3 that the solvent mixture can be represented entirely with continuous variables. The problem considered here is thus a nonlinear

programming problem (NLP).

3 SAFT-VR models for CO_2 + CH_4 + n-alkane mixtures

The asymmetric mixtures considered for the process, can exhibit surprisingly complex fluid phase behaviour. For example, mixtures of methane + hexane and longer n-alkanes exhibit regions of liquid-liquid separation close to the critical point of methane (Rowlinson & Swinton, 1982; McCabe, Gil-Villegas & Jackson, 1998); mixtures of CO_2 with long-alkanes also present liquid-liquid phase separation at low temperatures, and close to the critical point of CO_2 (Blas & Galindo, 2002; Galindo & Blas, 2002). In developing models to determine the thermodynamic properties and fluid phase behaviour of these systems it is crucial to incorporate the non-spherical nature of the molecules at at early stage, and in the case of mixtures involving CO_2, the effect of the multipolar (quadrupolar) interactions also needs to be taken into account.

Conventional approaches including cubic equations of state such as the Peng-Robinson equation (Peng & Robinson, 1976) or the Soave-Redlich-Kwong equation (Soave, 1972), and activity coefficient models such as that of Wilson (1964), the NRTL model (Renon & Prausnitz, 1968) and the UNIQUAC model (Abrams & Prausnitz, 1975), have been used widely for these systems, even though the underlying theories do not account explicitly for the molecular non-sphericity or electrostatic interactions. As a result, their main limitation is that they cannot be used with confidence as predictive tools and are therefore best suited for states within the range of available experimental data. In spite of these limitations, such methods find widespread and successful use in industry for conditions and systems for which there is ample experimental information. The use of G^E mixing rules (Huron & Vidal, 1979) in combination with the UNIFAC model to develop the more predictive equations of state, such as the PSRK (Holderbaum & Gmehling, 1991), has been shown to describe successfully the VLE of CO_2 +

methane and CO_2 + n-alkane binary mixtures provided temperature-dependent parameters are used (Keshtkar, Jalali & Moshfeghian, 1997). However, the PSRK EOS is found not be very accurate when mixtures of components of very different size are considered; in these cases modified size parameters have been presented to improve the accuracy of the approach (Li, Fischer & Gmehling, 1998). The VTPR EOS (Ahlers & Gmehling, 2001, 2002a) has been developed to overcome some of the weaknesses of the PSRK and has been shown to provide a good representation of the phase behaviour of the CH_4 + n-decane and the CO_2 + n-hexatriacontane binary mixtures (Ahlers & Gmehling, 2002b).

Other approaches based on a more detailed molecular model have been developed. The first-order perturbation theory (TPT1) of Wertheim (Wertheim, 1984a,b, 1986a,b, 1987; Müller & Gubbins, 2001; Paricaud, Galindo & Jackson, 2002; Tan, Adidharma & Radosz, 2008) and its implementation as an equation of state in the SAFT approach is one such example (Chapman, Gubbins, Jackson & Radosz, 1989, 1990). In SAFT-like approaches, molecular non-sphericity and directional interactions such as those involved in hydrogen bonding and aggregate formation (association), as well as dispersion interactions, are explicitly taken into account. In this work we use the SAFT-VR approach to model the mixtures of interest; the variable range capability of SAFT-VR makes it especially suited to treat systems with polar interactions. A description of the fluid is given through a set of parameters which have a physical meaning (representing the non-sphericity or the electrostatic interaction). Such molecular theories are more reliable than conventional approaches when it comes to the prediction of properties of systems where limited experimental data are available. Hence, they can be used as predictive tools with more confidence, particularly in high pressure regions (Wei & Sadus, 2000).

The SAFT-VR approach has powerful predictive capabilities. For instance, it provides an excellent representation of the properties of chain molecules such as n-alkanes (McCabe & Jackson, 1999) or polymers (Paricaud, Galindo & Jackson, 2004; McCabe, Galindo, Garcia-Lisbona & Jackson, 2001), and can also treat other complex molecules such as perfluoroalkanes (McCabe, Galindo, Gil-

Villegas & Jackson, 1998b). Of specific interest, the approach has been used in recent work (Galindo & Blas, 2002; Blas & Galindo, 2002) to model the entire homologous series of n-alkane + CO_2 mixtures, showing that the spectrum of phase behaviour, from vapour-liquid to vapour-liquid-liquid equilibria, is reproduced for these binary mixtures using a single parameter set. Such predictive capabilities permit the optimisation of both the generic solvent and process conditions over the entire feasible range, in contrast to more empirical models.

In SAFT-VR, a non-associating molecule i is described as a chain of m_i spherical segments, with the interaction between segments modelled by attractive potentials of variable range; the most common implementation, and the one used in this work uses square-well potentials to model the segment-segment interactions. Each segment is then characterised by its hard-core diameter σ_{ii} (here expressed in Å), the depth of the potential well ϵ_{ii}/k_B (in K), where k_B is the Boltzmann constant, and the range of the interaction λ_{ii} (in terms of the hard-core diameter). Since all the molecules considered in the CO_2 capture process are non-associating, the treatment of association need not be described here. Such capabilities will nevertheless be useful in the future to extend the range of compounds considered in the modelling of the natural gas stream, and in particular to the incorporation of water. The reader is referred to Patel, Paricaud, Galindo & Maitland (2003), Clark, Haslam, Galindo & Jackson (2006) and dos Ramos, Blas & Galindo (2007) for further details.

As for other equations of state, the intermolecular parameters used to describe the pure component and binary interactions within SAFT-VR are typically estimated from fluid phase experimental data. Properties of the relevant single component and binary mixture fluids have been intensively studied, both from experimental (Fredenslund & Mollerup, 1974; Hamam & Lu, 1974; Davalos, Anderson, Phelps & Kidnay, 1976; Brown, Kidnay & Sloan, 1988; Nagahama, Konishi, Hoshino & Hirata, 1974; Ohgaki & Katayama, 1977; Wei, Brown, Kidnay & Sloan, 1995; Somait & Kidnay, 1978; Kaminishi & Toriumi, 1968; Xu, Dong, Wang & Shi, 1992b; Bian, 1992; Xu, Dong, Wang & Shi, 1992a; Bian, Wang & Shi, 1993; Koonce & Kobayashi, 1964; Reamer, Olds, Sage & Lacey,

1942; Lavender, Sage & Lacey, 1940; Bett, Juren & Reynolds, 1968; Lin, Sebastian, Simnick & Chao, 1979; Reamer & Sage, 1963; Iwai, Hosotani, Morotomi, Koga & Arai, 1994; Inomata, Tuchiya, Arai & Saito, 1986; Jennings & Schucker, 1996; Chou, Forbert & Prausnitz, 1990; Nagarajan & Robinson, 1986; Sebastian, Simnick, Lin & Chao, 1980) and theoretical perspectives (McCabe, Galindo, Gil-Villegas & Jackson, 1998a; McCabe, Gil-Villegas & Jackson, 1998; Galindo & Blas, 2002; Blas & Galindo, 2002; Nguyen-Huynh, Tran, Tamouza, Passarello, Tobaly *et al.*, 2008), but experimental data for ternary mixtures (Dunyushkin, Skripka & Nenartovich, 1977) are scarce for the systems of interest here. Thus, we first present the SAFT-VR molecular models developed for this work; we obtain transferable binary interaction parameters where necessary and compare the result of the SAFT-VR calculations for the phase equilibria of pure components and binary mixtures to experimental data. Subsequently, we examine the predictive capabilities of the EOS. We compare the VLE calculations performed with SAFT-VR to experimental data for binary mixtures involving a wide range of n-alkanes, different to those used to determine the binary interaction parameters, and for the ternary system of interest.

3.1 Pure component models

The molecular models for CO_2 and CH_4 used in this work are based on those presented in (Galindo & Blas, 2002; Blas & Galindo, 2002). The CO_2 molecule is modelled as two tangentially bonded spheres ($m_i = 2$) and CH_4 as a single spherical core ($m_i = 1$). Both components are treated as non-associating. The parameters characterising the segment-segment square-well interaction (σ_{ii}, ϵ_{ii}/k_B and λ_{ii}) for CO_2 and CH_4 have been estimated in previous work using experimental vapour pressure and saturated liquid density data from the triple point to about 90 % of the critical temperature. In common with other classical equation of state approaches, this procedure leads to an overprediction of the critical pressure and temperature (Galindo & Blas, 2002; Paricaud, Galindo & Jackson, 2004) since the long-range correlations characteristic of the critical re-

gion are not treated. In this work, however, the near- and super-critical regions of these two compounds are of special interest. Hence, in order to reproduce the critical temperature and pressure accurately, the size and energy parameters σ_{ii} and ϵ_{ii}/k_B have been rescaled (see Galindo & Blas (2002) and Blas & Galindo (2002) for more detail). The resulting parameters are presented in table 1; the unscaled parameters are also presented for completeness.

Good estimates of the molar volume of the vapour and liquid states are necessary for the simulation of the separation process, for instance to convert mass flow rate into volumetric flow rate, or to estimate the absorber or tank volume. An assessment of the description of the molar volume V by comparison with the experimental data is presented for supercritical conditions as well as for the vapour-liquid equilibrium region. We present pressure-volume PV isotherms from 273K to 400K for CH_4 in figure 2, and from 273K to 411K for CO_2 in figure 3. In both cases, the agreement between the SAFT-VR predictions and experimental data is seen to be reasonably good.

An n-alkane (component a) with N_a carbon atoms is modelled as a chain of $m_a = (N_a - 1)/3 + 1$ segments (Jackson & Gubbins, 1989; Galindo, Whitehead, Jackson & Burgess, 1996). For the n-alkane homologous series, a correlation proposed by Paricaud, Galindo & Jackson (2004), which gives the SAFT-VR parameters as a function of the molecular weight of n-alkane a is used:

$$MW_a/(\text{g.mol}^{-1}) = 14 \times N_a + 2, \tag{2}$$

$$m_a = 0.02376 \times MW_a/(\text{g.mol}^{-1}) + 0.6188, \tag{3}$$

$$m_a(\sigma_{aa}/\text{Å})^3 = 1.53212 \times MW_a/(\text{g.mol}^{-1}) + 30.753, \tag{4}$$

$$m_a(\epsilon_{aa}/k_B)/\text{K} = 5.46587 \times MW_a/(\text{g.mol}^{-1}) + 194.263, \tag{5}$$

$$m_a\lambda_{aa} = 0.04024 \times MW_a/(\text{g.mol}^{-1}) + 0.6570, \tag{6}$$

where MW_a is the molecular weight of n-alkane a in g.mol^{-1}.

The representation of the intermolecular parameters of the entire n-alkane series by simply changing the number of carbon atoms, N_a, makes it possible to optimise the n-alkane as part of the CAMPD problem. Importantly, blends

of n-alkanes are modelled by using a non-integer number of carbon atoms; this idea is equivalent to the lumping techniques used to model oil fractions which is based on the ubiquitous principle of congruence (Brønsted & Koefoed, 1946; Rowlinson & Swinton, 1982). Thus, solvent blends are represented by the continuous variable N_a, and a mixture of CO_2, CH_4 and several n-alkanes is treated as a pseudo-ternary mixture. The assumption is justified by considering that since the chain length of the solvent tends to be relatively high, the partial pressure of the solvent is low, especially at elevated pressures. This means that the relative composition of the components in the solvent (akin to the polydispersity) is not expected to greatly affect the vapour-liquid equilibria of CO_2/CH_4 in the solvent. The greatest impact of this assumption is likely to be on solvent loss in the CO_2 waste stream, as this corresponds to the location in the process where the pressure is lowest.

3.2 Binary intermolecular interaction parameters

In order to model the thermodynamic properties of binary mixtures with the SAFT-VR approach, combining rules must be applied to describe the interaction between the two different species, i and j (Galindo, Davies, Gil-Villegas & Jackson, 1998). These unlike ('cross') intermolecular interaction parameters are often obtained by means of the pure component parameters following the so-called Lorentz-Berthelot (arithmetic and geometric, respectively) rules, so that for our square-well parameters,

$$\sigma_{ij} = \frac{\sigma_{ii} + \sigma_{jj}}{2}; \qquad \epsilon_{ij} = (1 - k_{ij}^{\epsilon})\sqrt{\epsilon_{ii}\epsilon_{jj}}; \qquad \lambda_{ij} = (1 - k_{ij}^{\lambda})\frac{\sigma_{ii}\lambda_{ii} + \sigma_{jj}\lambda_{jj}}{\sigma_{ii} + \sigma_{jj}}. \quad (7)$$

For the case of hard core potentials, the arithmetic mean used to determine σ_{ij} is exact, but the Berthelot geometric mean for $\epsilon_{ij} = \sqrt{\epsilon_{ii}\epsilon_{jj}}$ and the arithmetic mean for λ_{ij} often fail for for non-ideal systems, leading to inaccurate predictions, and in extreme cases, to the wrong type of phase behaviour. Adjustable correction factors or binary interaction parameters k_{ij}^{ϵ} and k_{ij}^{λ} are commonly introduced to provide a good representation of the fluid mixture.

Although new combining rules have been proposed which improve on the description of the traditional Lorentz-Berthelot expressions (Haslam, Galindo & Jackson, 2008), in order to obtain the best possible agreement with experimental data for the conditions of interest in the process, we estimate the unlike interaction energy parameters k_{ij}^{ϵ} using isothermal vapour-liquid equilibrium experimental data over a wide range of temperatures and pressures for three relevant binary mixtures: CO_2 + CH_4, CO_2 + C_{10}, and CH_4 + C_{10}. The relatively long chain n-decane (C_{10}) is chosen as a representative compound in the n-alkane series as large sets of experimental data are available for this molecule, including data for the ternary CO_2 + CH_4 + C_{10} mixture. We find that an adjustment in only k_{ij}^{ϵ} is required to obtain a good description of the phase behaviour of the mixtures of interest; the unlike range parameter k_{ij}^{λ} is 0 throughout.

A large number of experimental data points and sources are used for the estimation of k_{ij}^{ϵ} for each binary mixture. For CO_2 + CH_4 mixtures, we use 317 experimental data points over 24 temperatures (Fredenslund & Mollerup, 1974; Hamam & Lu, 1974; Davalos, Anderson, Phelps & Kidnay, 1976; Brown, Kidnay & Sloan, 1988; Nagahama, Konishi, Hoshino & Hirata, 1974; Ohgaki & Katayama, 1977; Wei, Brown, Kidnay & Sloan, 1995; Somait & Kidnay, 1978; Kaminishi & Toriumi, 1968; Xu, Dong, Wang & Shi, 1992b; Bian, 1992; Xu, Dong, Wang & Shi, 1992a; Bian, Wang & Shi, 1993). For CO_2 + C_{10} and CH_4 + C_{10}, we selected experimental data for pressures below 10 MPa and temperatures below 477 K. This corresponds to the operating range of the separation process that is being considered in our work. All of the experimental data available in the Detherm database (Fletcher, F., McMeeking & Parkin, 1996) are used for CH_4 + C_{10} (111 points) (Koonce & Kobayashi, 1964; Reamer, Olds, Sage & Lacey, 1942; Lavender, Sage & Lacey, 1940; Bett, Juren & Reynolds, 1968; Lin, Sebastian, Simnick & Chao, 1979) and for CO_2 + C_{10} (85 points) (Reamer & Sage, 1963; Iwai, Hosotani, Morotomi, Koga & Arai, 1994; Inomata, Tuchiya, Arai & Saito, 1986; Jennings & Schucker, 1996; Chou, Forbert & Prausnitz, 1990; Nagarajan & Robinson, 1986; Sebastian, Simnick, Lin &

Chao, 1980), both over 15 temperature values (see table 2).

Each binary k_{ij}^{ϵ} parameter is estimated by minimising a least-squares objective function, $F(k_{ij}^{\epsilon})$

$$F(k_{ij}^{\epsilon}) = \frac{1}{N_{exp}} \sum_{i=1}^{N_{exp}} (P_{EXP}(i) - P_{SAFT}(i; k_{ij}^{\epsilon}))^2 + (y_{EXP}(i) - y_{SAFT}(i; k_{ij}^{\epsilon}))^2, \tag{8}$$

where N_{exp} is the total number of data points (a data point corresponds to a specific combination of temperature T and liquid mole fraction x, $P_{EXP}(i)$ is the experimental pressure in MPa for the ith data point, $y_{EXP}(i)$ is the vapour mole fraction for the ith data point, $P_{SAFT}(i; k_{ij}^{\epsilon})$ and $y_{SAFT}(i; k_{ij}^{\epsilon})$ are the equilibrium pressure (in MPa) and vapour mole fraction calculated using SAFT-VR with the given value of k_{ij}^{ϵ}, the fixed set of pure component parameters, and the values of x and T for the ith data point. The minimisation of the objective function $F(k_{ij}^{\epsilon})$ with respect to the binary interaction parameter k_{ij}^{ϵ} is then performed using the parameter estimation functionality of gPROMS (Process Systems Enterprise Ltd, 2008). In assessing the models developed in this way, relative errors in the predicted pressure and absolute errors in the vapour mole fraction are reported. They are calculated as follows

$$\%\text{ADD}P = \frac{1}{N_{exp}} \sum_{i=1}^{N_{exp}} \left| \frac{P_{SAFT}(i) - P_{EXP}(i)}{P_{EXP}(i)} \right| \times 100, \tag{9}$$

$$\text{AAD}y = \frac{1}{N_{exp}} \sum_{i=1}^{N_{exp}} |y_{SAFT}(i) - y_{EXP}(i)| . \tag{10}$$

The values of the binary interaction parameters obtained for each mixture are shown in table 2. Information about the experimental data used and the errors between the predicted and experimental values of pressure and vapour mole fraction are also reported. Very good agreement is obtained between the experimental data and the SAFT-VR calculations, with a percentage average absolute deviation in pressure of less than 10% and an average absolute deviation in gas mole fraction of less than 0.024 for all three binary mixtures, over a wide range of temperature and pressure conditions. This can be seen further in figures

4, 5 and 6, where pressure-composition phase diagrams are shown for the three binary mixtures examined to develop the parameters. These phase diagrams are plotted at several temperatures for each mixture. The data available for the CH_4 + CO_2 mixture are at low temperatures, where the VLE region is largest, and the quality of fit is seen in figure 4 to improve as the temperature increases and approaches realistic process temperatures. The *n*-decane + CO_2 mixture yields the largest deviation in terms of pressure. It can be seen in figure 6 that this is due to an overestimation of the critical point, especially at the highest temperature.

3.3 Prediction of mixture phase behaviour

One of the advantages of SAFT-VR is that it may be used in a transferable manner within a homologous series, as shown by Blas and Galindo specifically in the case of CO_2 + n-alkane mixtures (Galindo & Blas, 2002; Blas & Galindo, 2002). This is in part due to the definition of intermolecular interactions in terms of inter-segment interaction potentials. It is useful to recall that the CH_4 molecule is represented by a single segment described by the parameters listed in table 1, and the *n*-decane molecule by several identical segments with parameters given by equations (2)-(6). The interaction parameters in table 2 are therefore segment-segment parameters. We assume that the interaction parameters between CH_4 (or CO_2) and *any* *n*-alkane solvent or solvent blend are the same as those between CH_4 (or CO_2) and C_{10}, so that

$$k^{\epsilon}_{CH_4,N_a} = -0.053006; \tag{11}$$

$$k^{\epsilon}_{CO_2,N_a} = +0.089642, \tag{12}$$

where N_a denotes the average carbon number of the *n*-alkane mixture.

Predictive calculations have been carried out for the mixtures with *n*-hexadecane, CH_4 + C_{16}, and CO_2 + C_{16}. Constant temperature, pressure-composition Pxy phase diagrams are plotted in figure 7 for CH_4 + C_{16} and in figure 8 for CO_2 + C_{16}. Both mixtures are well represented by the SAFT-VR thermodynamic

model developed, particularly considering that the unlike interaction parameters were estimated using the corresponding mixtures with n-decane. We also show predictions for a range of n-alkanes including(n-hexane (C_6), n-octane (C_8), n-dodecane (C_{12}) and n-hexadecane (C_{16})) at 313.15 K; the results are presented in figure 9 for CO_2 mixtures, and in figure 10 for CH_4 mixtures. It is gratifying to see such a good predictive capability using our transferable parameters within the SAFT-VR approach. The expected onset of liquid-liquid equilibria is seen at high pressure for the mixtures with the longer hydrocarbons (Galindo & Blas, 2002) (cf. CO_2 + C_{16} in figures 8 and 9).

Once the parameters for the binary mixtures have been obtained, the SAFT-VR approach can be used predictively for ternary mixtures, without any further adjustment or estimation of parameters. This predictive capability is useful since very few experimental data involving ternary mixtures of CO_2, CH_4 and an n-alkane can be found in the literature (Dunyushkin, Skripka & Nenartovich, 1977); these are isothermal data at 344.15 K, and at four pressures: $\sim$ 5, 10, 15 and 20 MPa. In figures 11 a) to d) the SAFT-VR predictions are compared with these experimental data and very good agreement is seen between the theory and the experiments. We find that the SAFT-VR model performs better for pressures below 10 MPa, which can be expected, since the experimental data used in the fitting of the binary interaction parameters was restricted to this range. However, the model still performs very well for pressures beyond 10 MPa. It may also be observed from the orientation of the vapour-liquid coexistence tie-lines in figure 11 that, for a gas mixture of CO_2 and CH_4 in contact with a heavier hydrocarbon solvent such as C_{10}, a preferential absorption of CO_2 in the solvent takes place.

4 Process and economic modelling

In this section, we present the assumptions made in the process and economic models, used to develop the detailed formulation of the CAMPD problem.

4.1 Process model

Steady-state mass and energy balances for all the units in the flowsheet (figure 1) have been derived. In developing steady-state models of each unit, thermodynamic equilibrium and complete mixing are assumed where relevant. Mass-transfer limitations are not modelled explicitly, but are taken into account in the sizing of the absorber through an overall efficiency factor. It is assumed that there are no thermal losses. This level of detail is sufficient to obtain cost estimates to compare different design options. Expansion valves are used to reduce the pressure of a gas or of a liquid and are assumed to be isenthalpic. The pump is assumed to operate isentropically. In the flash unit, we assume that the liquid outlet stream and the vapour outlet stream are completely separated so that there is no liquid carry-over in the gas stream or gas bubbles in the liquid stream. The equations for the mass and energy balances of each unit are straightforward and can be found in Keskes (2007). The thermodynamic properties such as the enthalpies and entropies are calculated using the SAFT-VR equation of state. This is done based on the overall composition of each phase considered so that no assumption of ideal mixing is necessary. The calculation of the phase equilibrium is the most challenging aspect of the process model and is described in the remainder of this section.

In computing the phase equilibrium, we ensure that the crystallisation of the hydrocarbon solvent, regions of liquid-liquid immiscibility, and three-phase separation are avoided by constraining the operating conditions of the process. All streams in the process are thus assumed to consist of up to two phases, except for the outlets of the flash unit and of the absorber trays, which are liquid or vapour streams by design. This does not lead to any loss of generality: if the conditions in the flash unit result in a purely liquid phase, the flowrate of the gas outlet stream is set to zero and all the material exits as a liquid stream. The ability for other streams to contain one or two phases is modelled by adopting the 'virtual equilibrium' or 'negative flash approach' (Whitson & Michelsen, 1989). This is applicable when vapour-liquid equilibrium is possible from a

total composition at the specified pressure and temperature. The application of this approach in the context of process simulation has been discussed by Müller & Marquardt (1997), where it was found to be very efficient and to provide a correct, albeit not guaranteed, solution for many cases. The existence of two virtual phases is assumed throughout the process, and the phase fractions of the virtual liquid phase a^* and the virtual vapour phase b^* are allowed to take values that are greater than 1 or less than 0. The virtual equilibrium problem is then described by the equality of chemical potentials and pressures between the two virtual phases:

$$\mu_i^{liq}(X^*, V^{liq}, T^{spec}, N_a) = \mu_i^{vap}(Y^*, V^{vap}, T^{spec}, N_a), \qquad i = 1, ..., nc, \tag{13}$$

$$P^{liq}(X^*, V^{liq}, T^{spec}, N_a) = P^{vap}(Y^*, V^{vap}, T^{spec}, N_a) = P^{spec}, \tag{14}$$

$$Z^{spec} = a^* X^* + b^* Y^*, \tag{15}$$

and

$$a^* + b^* = 1, \tag{16}$$

where X^* and Y^* are the vectors of mole fraction in the liquid and vapour, respectively, in the virtual equilibrium. μ_i^{liq} and μ_i^{vap} are the chemical potentials of component i in the liquid and vapour phases respectively, nc is the number of components in the mixture, V^{liq} and V^{vap} are the molar volumes of the liquid and vapour phases respectively, P^{liq} and P^{vap} the pressures of the liquid and vapour phases respectively, P^{spec} the specified pressure, T^{spec} the specified temperature, and Z^{spec} the vector of specified overall mole fractions. The chemical potentials and pressures are calculated with the SAFT-VR equation.

Depending on the values of a^* obtained, there are three different scenarios that can be used to determine the value of a, the phase fraction of the liquid phase in the real system:

1. $a^* > 1$: subcooled liquid $\rightarrow a = 1$
2. $a^* < 0$: superheated vapour $\rightarrow a = 0$
3. $0 \leq a^* \leq 1$: coexistence $\rightarrow a = a^*$

The true phase fractions for liquid phase, a, and the vapour phase, b, and the true mole fractions of the liquid phase, X, and the vapour phase, Y, may be obtained by defining binary variables and appropriate constraints to represent each scenario. In practice, we have found it to be sufficient to express this through non-differentiable constraints:

$$a = a^* H(a^*) + (1 - a^*) H(a^* - 1) \tag{17}$$

where $H()$ denotes the Heaviside function,

$$X = X^* + \frac{1}{2}(|b^*| - b^*)(X^* - Y^*), \tag{18}$$

$$Y = Y^* + \frac{1}{2}(|a^*| - a^*)(Y^* - X^*), \tag{19}$$

and

$$a + b = 1. \tag{20}$$

4.1.1 Sizing and economic modelling

The net present value (NPV) of the process, based on a given process life and interest rates, can be used as an economic objective function. This requires an estimate of the purchased cost of each unit, which can then be used to calculate the total capital investment (TCI) for the plant. Costs associated with the operation of the plant (total operating costs, TOC) also need to be estimated, including labor, utilities, maintenance, repairs, and taxes.

The dimensions of each unit can be estimated based on the flow characteristics and energy duty where relevant. The process model discussed in the previous section is used to estimate the composition, flowrate, and properties for each stream in the process, as well as the energy requirement of the pump. This in turn can be used to determine the capital and operating costs, as documented in standard texts (Douglas, 1988; Perry, Green & Maloney, 1997).

To calculate TCI, the purchased cost is obtained for a given material of construction, for instance carbon steel (CS), and a material factor must be applied if a more complex material needs to be used. The installation costs are

generally higher than the purchased cost and should be taken into account in the total capital investment. They include the piping, instrumentation, electrical, civil work, structures and building, and lagging. The installation cost of the equipment is obtained by applying a multiplicative factor to the purchase cost. This factor depends on the equipment type and cost. Finally, indirect costs and working capital need to be estimated in order to obtain the total capital investment. Indirect costs include the cost of engineering and supervision, construction expenses, contractors' fees, and contingency.

In order to determine the TOC, the following contributions are taken into account: personnel costs (labour and supervision) to operate the plant, the cost of raw materials such as the solvent, indirect expenses such as depreciation and taxes, insurance, maintenance, royalties, and non-manufacturing costs (e.g., administration and R&D costs). Total operating costs can be divided into direct operating costs, fixed charges, and plant overhead. The direct operating costs are estimated based on the material and energy flows in the process. Other costs depend on the type and size of the equipment used.

Finally, the revenue is obtained by calculating the value of the natural gas sales. Details of the calculation of the TCI, the TOC and the revenue, present value gas sales, $PV_{gas-sales}$, can be found in the Appendix.

To obtain a profit function, the NPV of the operating costs and revenue must be calculated. There are significant uncertainties surrounding both natural gas prices and interest rates. Since both have the potential to rise, changes in these figures are assumed to offset each other. The sale gas price is set as 6 USD/million BTU, representative of the level of the NYMEX natural gas index over the past five years (FT, 2009), and the interest rate at 0%. The plant life is considered to be 15 years. The total operating costs, PV_{opex}, over the life of the project, n_{year}, are then calculated as

$$PV_{opex} = \text{TOC} \times n_{year}, \tag{21}$$

The total separation cost $SepCost$ for the project is then given by

$$SepCost = PV_{opex} + \text{TCI}. \tag{22}$$

Finally, we can then calculate a simple estimate of the total profit of the plant as,

$$NPV = PV_{gas-sales} - SepCost. \tag{23}$$

5 Case study: CAMPD for CO_2 capture from natural gas

5.1 Problem specification

The design problem is defined as follows. For the flowsheet shown in figure 1, with a feed flowrate of 1 kmol.s^{-1}, at 7.96 MPa and 301 K (Anderson & Siahaan, 2005), and a given composition, find the values of the design variables:

- average carbon number of the n-alkane solvent blend, N_a,
- solvent flowrate, F_S,
- temperature of the inlet gas stream to the absorber, $T_{A,IN}$,
- absorber pressure, P_A,
- flash unit pressure, P_F,

that maximise a chosen performance objective, and meet the following design specifications and constraints

- the average n-alkane carbon number N_a must be between 7 and 14,
- the height H of the absorption column must be less than 50 m,
- the cross-sectional area A_t of the absorption column must be less than 30 m^2,
- the solvent viscosity in the column μ_{L,N_a} must be less than 100 cP,
- the gas inlet temperature into the absorption column, TC_{IN}, must be between 273.15K and 500K,

- the temperature at every point in the process (represented by the vector T_p) must be at least 5K greater than the melting temperature of the solvent, ($T_{SOLID}(N_a)$), to avoid solidification of the solvent,
- the mole fraction of CH_4 in the sales gas outlet stream ($x_{CH_4,OUTLET}$) must be greater than 97%,
- the pressure of the waste CO_2 stream must be equal to 0.1MPa
- the theoretical number of trays in the absorber is fixed to 10 $N_{theoretical} = 10$.

The bounds on N_a have been chosen to make sure that the n-alkane solvent is within its liquid range over the range of operating conditions. Throughout, the process, the temperature is constrained to be 5 degrees above the melting temperature of the solvent, to avoid solidification in the process. The melting temperature T_m (in K) is obtained from a simple correlation produced in this work where $T_m = 10.92N_a + 128$.

Process/solvent optimisations are carried out at feed compositions of 10 and 70 mol% CO_2, to cover the spectrum of compositions that may be expected in natural gas feeds. An intermediate value of 30 mol% CO_2 is also included, corresponding to the level of CO_2 in the natural gas for the Grissik case study (Anderson & Siahaan, 2005). We consider two performance objectives: the NPV of the profit over a 15 year lifetime and the extent of separation as measured by the purity (CO_2 mole fraction) of the waste gas stream. The purity constraint on the sale gas stream ensures that this stream is always at least 97% pure in methane. Depending on the ease of separation, inlet conditions, and the marginal cost of producing one unit of sale gas, there may be a trade-off between these two objectives. This work considers only a simple process flowsheet, which is likely to have a less than optimal separation performance, but will also have a low cost. 'Separation performance' refers to the purities of *both* gas outlet streams. A constraint is imposed on the purity of the sale gas stream but not on that of the waste gas stream. An improved separation performance

could, for example, reduce the quantity of methane lost to the waste gas stream. Increasing the complexity of the process flowsheet is likely to improve this separation performance, but will also increase costs. In the case of this flowsheet, it is found that there is almost no trade-off between the objectives of separation performance and maximal NPV. This is due to the few degrees of freedom available in the optimisation of the process conditions for such a simple flowsheet. The constraint on the purity of the sale gas stream is such that whether the objective be maximal NPV or separation performance, the optimal conditions are those corresponding to a sale-gas stream that is at least 97% pure in methane. Optimisations are therefore carried out with an objective of maximal NPV. Equivalent results would be obtained through an objective of separation performance.

The model is implemented in gPROMS (Process Systems Enterprise Ltd, 2008) in a modular fashion, allowing units to be added and removed easily. The SAFT-VR calculations are implemented in Fortran90 and accessed via a Foreign Object interface (Kakalis, Kakhu & Pantelides, 2004; Kakalis, 2006). Since N_a is treated as a continuous variable, this problem is a non-linear programming (NLP) problem, which can be solved with the successive quadratic programming solver in gPROMS (Process Systems Enterprise Ltd, 2008).

5.2 Optimal process performance

The results of the optimisations are reported in table 3. The solution time on a Pentium 1.7 GHz processor ranges from 20 CPU seconds for the 10% CO_2 scenario to 100 CPU seconds for the 70% CO_2 scenario, and requires 10 to 30 iterations of the NLP solver. Firstly, it is important to point out that even for this most basic flowsheet, the process succeeds in separating CH_4 from a mixed stream of CH_4 and CO_2, producing a purity in the CH_4 stream of 97% for all feed compositions. Secondly, all this is achieved with a positive NPV for the separation process. One should also note, however, that the cost of extracting the natural gas from the reservoir has not been considered. Nevertheless, for this

process, the costs of the separation are small compared to the revenue generated by gas sales. These low costs are partly due to a low energy requirement of the process. Further work on the design of the process flowsheet would improve the estimated NPV, mainly by reducing the quantity of CH_4 lost to the waste gas stream, through improvement of the separation performance. However, any increase in process complexity must be accompanied by an increase in process performance that is large enough to offset the additional capital and operating costs incurred.

The NPV of the process is significantly higher for the lower CO_2 concentration inlets. This is unsurprising since there is a greater quantity of CH_4 entering the process, and therefore, even with low separation performance, there is a larger amount of CH_4 leaving in the sale gas stream i.e., a larger sale gas flow rate. The absorption column height lies at its upper bound of 50m for the 10% CO_2 inlet concentration. Performance could therefore be improved upon modification of the flowsheet.

The separation of the two gases occurs because of physical absorption. The three different inlet stream scenarios demand different levels of separation; the 10% CO_2 scenario requires the removal of much less CO_2 than the 70% scenario, in order to arrive at a sale gas purity of 97% in CH_4. This difference is reflected in the optimal process conditions shown in table 3. The optimisation variables (absorber pressure, solvent flowrate and solvent chain length) differ considerably between these two extremes of inlet composition.

The absorption conditions may be altered by controlling the pressure inside the absorber and the solvent flowrate, which will alter the global composition of the mixture. The temperature and pressure in the absorber are linked since any expansion of the gas before the absorption column will lead to a change in its temperature. The temperature of the process is also affected by the expansion of the bottom stream from the absorber into the flash drum, which operates at atmospheric pressure. Finally, the mixing of the solvent and the gas stream is exothermic. The column cross section and flash drum volume are linked to both the pressure and the solvent recirculation rate. A higher pressure results

in reduced equipment volumes, as does a reduced solvent flowrate. The solvent losses into the gas outlet streams are small, of the order of 1000 kmol.yr^{-1}.

The 70% scenario operates at a higher pressure, a lower solvent flowrate, and with a shorter n-alkane as solvent. The combination of these factors allows access to the low temperature, high pressure area of the ternary fluid phase diagram in which it is possible to dramatically reduce the CO_2 content of the vapour phase. This allows for the required purity threshold to be attained in the available ten theoretical stages. While these conditions produce a sale-gas stream of the required purity, the recovery of methane is the lowest of all the scenarios. This is because the phase behaviour at these low temperature-high pressure conditions does not produce large phase splits. Therefore, the quantity of methane remaining in the liquid stream at the bottom tray of the absorber is relatively high. In addition, in order to operate at these low temperatures, the flowrate of solvent must be low. The enthalpy of mixing between the solvent and gas streams increases significantly with the quantity of solvent flowing around the column. This is the reason for the higher process temperatures in the 10% and 30% scenarios. In this very simple flowsheet the temperature has to be reduced though a reduction in the absorption column pressure. This is not feasible for the 70% scenario, since both a low temperature and a high pressure are required for the optimal phase behaviour to be accessed. The optimal solvents in the 10% and 30% cases are very similar, while for the 70% case the optimal solvent is much shorter. Again, the optimal solvent chain length involves a trade-off, since the longer alkanes absorb CO_2 more effectively, but also solidify at higher temperatures. The solvent chain length of 9.3 in the 70% case reflects this, since operation at such low temperatures would not be possible with a longer solvent.

The scenarios with lower CO_2 inlet concentrations (10% and 30%) lead to similar optimal process and solvent parameters. The separation is easier in these cases, and therefore it is possible to take advantage of the wider phase splits obtained at higher temperatures and lower pressures. This reduces the mole fraction of CH_4 absorbed into the liquid phase. More stages are required in

this area of the fluid phase diagram to achieve the necessary purity threshold, and therefore with the 70% scenario one is not able to take advantage of this strategy.

A consequence of the use of the principle of congruence is that solvent components with chain lengths shorter than the blend average have a higher partial pressure, and are therefore present in larger quantities in the vapour phase. This may result in an underestimation of the solvent losses. To quantify, we may examine a worst-case scenario for the most polydisperse solvent blend. Upon going from an average representation of a blend to the explicit modelling of two components, the greatest relative difference in n-alkane composition in the vapour phase is found at the lower bound of the flash drum atmospheric pressure. At these conditions, a monodisperse solvent of chain length $N_a = 10$ would be present in the vapour phase at a mole fraction of around 10^{-5}. However, a C7/ C14 blend with an average chain length of 10 would have a vapour phase mole fraction of the order of 10^{-4}. The flowrate of the CO2 waste stream is around 500 mol.s^{-1}. Solvent losses from this stream due to polydispersity would consequently be increased by a factor of 10, to around 5x10^{-2} mol.s^{-1}. This translates to a fresh solvent cost of around \$100,000/yr, although this lost solvent could subsequently be recovered as a liquid upon compression of the CO_2 waste stream for transportation and storage. This indicates that the treatment of the blend as a single n-alkane is justified for this stage of the design process.

Since it is possible to design economically viable processes with such a basic flowsheet over a wide range of feed conditions, the use of n-alkane solvents provide a promising alternative for methane recovery. The suitability of such solvents has been further investigated by replacing some of the methane in the feed by ethane, so that the ethane feed mole fraction is 5%. In this case, the basic flowsheet leads to the desired separation for all CO_2 concentration scenarios, with a small decrease in NPV as most of the ethane is lost in the CO_2 waste stream (Keskes, 2007).

Clearly, a more complex flowsheet would provide more flexibility in process conditions and would increase the profitability of the process. For example, the

addition of cooling to the process would decouple the temperature and pressure in the absorber, allowing one to operate the process at high pressure-low temperature states while maintaining a high solvent recirculation rate. The addition of absorption stages would also add flexibility, and in particular, the use of multiple columns in series, at different conditions, would allow multiple absorption strategies to be employed. For example, with the first column one could exploit the ability of the high pressure-low temperature phase behaviour to remove bulk quantities of CO_2, while the conditions in a second column could be tuned to reduce CH_4 losses to the liquid phase. The use of a predictive equation of state, such as SAFT-VR, to determine the thermodynamic properties, and therefore the phase behaviour, means that the domain of the process optimisation may span the entire range of feasible operating conditions. The predictions of this EOS may be treated with confidence, in any part of the fluid phase region. The optimisation constraints are purely physical ones, for example, remaining above the solidification temperature of the solvent, or restricting the size of the units.

6 Conclusions

In this work, we have presented a computer-aided molecular and process design (CAMPD) methodology based on the SAFT-VR equation of state. We have applied this to the separation of CO_2 and CH_4 through physical absorption of the CO_2 into an n-alkane solvent. The approach can be used to identify the optimal solvent blend and operating conditions. As part of the methodology, a predictive thermodynamic model of the pseudo-ternary mixture (CH_4 + CO_2 + C_n blend) with the SAFT-VR EOS has been constructed, which provides a good description of the experimental data. A simple process model has been developed for a basic flowsheet, and an economic model has also been presented. The overall optimisation problem has been implemented in gPROMS, with design studies undertaken to assess technical feasibility and economic performance using three inlet stream compositions. The potential for separation has been investigated based on a purity/NPV objective. We find that, even with this

most basic flowsheet, one process is capable of achieving a high purity CH_4 stream (97% pure in CH_4) with a high CO_2 enrichment ratio from the input stream to the waste gas stream and a positive NPV. This is true of all of the inlet concentrations considered.

We have also demonstrated the benefits of employing an advanced equation of state within a process modelling and optimisation framework. Since a physical absorption process is centered around high-pressure fluid phase behaviour, accurate thermodynamic predictions are a crucial part of any valid process model. The use of SAFT-VR facilitates this, even under highly non-ideal, high-pressure conditions.

The results obtained indicate that physical absorption into an n-alkane is a promising approach for CO_2 capture from high-pressure natural gas streams. In all cases, profits through gas sales far outweigh capital and operating costs. The flowsheet layout was not optimised in this study and there is likely to be additional scope for improving the performance of the process as has been shown in a preliminary study (Pereira, Keskes, Galindo, Jackson & Adjiman, 2008). We are currently developing this further, as well as considering a wider range of components in the inlet gas stream. The screening of solvents outside the n-alkane family may also improve the performance of the process. A group contribution equation of state, such as SAFT-γ (Lymperiadis, Adjiman, Galindo & Jackson, 2007; Lymperiadis, Adjiman, Jackson & Galindo, 2008), would be particularly valuable in modelling more complex solvents and is also a focus of our current work. The inclusion of a wider range of solvents will require the introduction of discrete decisions in the problem formulation. Finally, although different inlet concentrations of the CO_2 have been considered, different processes (equipment sizes) have been designed for each feed. Given that large variations in CO_2 content are expected over the lifetime of a field, it would be useful to develop a robust process, using techniques for design under uncertainty e.g., Mohideen, Perkins & Pistikopoulos (1996).

Acknowledgements

E.K. and F.E.P. are grateful to Schlumberger Cambridge Research and the Engineering and Physical Sciences Research Council (EPSRC) of the UK, respectively, for PhD studentships. Additional funding from the EPSRC (grants GR/T17595, GR/N35991, GR/R09497, and EP/E016340), the Joint Research Equipment Initiative (JREI) (GR/M94427), and the Royal Society-Wolfson Foundation refurbishment grant is also acknowledged.

References

Abrams, D. S., & Prausnitz, J. M. (1975). Statistical thermodynamics of liquid mixtures: A new expression for the excess Gibbs energy of partly or completely miscible systems, *AIChE J.*, *21*, 116.

Ahlers, J., & Gmehling, J. (2001). Development of an universal group contribution equation of state I. Prediction of liquid densities for pure compounds with a volume translated Peng-Robinson equation of state, *Fluid Phase Equilib.*, *191*, 177.

Ahlers, J., & Gmehling, J. (2002a). Development of a universal group contribution equation of state. 2. Prediction of vapor-liquid equilibria for asymmetric systems, *Ind. Eng. Chem. Res.*, *41*, 3489.

Ahlers, J., & Gmehling, J. (2002b). Development of a universal group contribution equation of state III. Prediction of vapor-liquid equilibria, excess enthalpies, and activity coefficients at infinite dilution with the VTPR model, *Ind. Eng. Chem. Res.*, *41*, 5890.

Anderson, C. L., & Siahaan, A. (2005). Case Study: Membrane CO_2 removal from natural gas, Grissik gas plant, Sumatra, Indonesia, *55th Annual Oklahoma University Laurance Reid Gas Conditioning Conference*, p. 71.

API (1989). American Petroleum Institute specification for oil and gas separators: API 12J-1989.

Bardow, A., Steur, K., & Gross, J. (2010). Continuous-molecular targeting for integrated solvent and process design, *Ind. Eng. Chem. Res.*, *49*, 2834.

Beaudoin, J. M., & Kohn, J. P. (1967). Multiphase and volumetric equilibria of the methane-n-decane binary system at temperatures between -36 and 150°C, *J. Chem. Eng. Data*, *12*, 189.

Bett, K. E., Juren, B., & Reynolds, R. G. (1968). *Physical properties of liquids and gases for plant and process design: Proceedings of a Symposium*, pp. A53–A76.

Bian, B. (1992). *Measurement of Phase Equilibria in the Critical Region and Study of Equations of State*, Ph.D. thesis, University of Nanjing.

Bian, B., Wang, Y., & Shi, J. (1993). Simultaneous determination of vapor-liquid equilibrium and molar volumes for coexisting phases up to the critical temperature with a static method, *Fluid Phase Equilib.*, *90*, 177.

Blas, F. J., & Galindo, A. (2002). Study of the high pressure phase behaviour of CO_2+n-alkane mixtures using the SAFT-VR approach with transferable parameters, *Fluid Phase Equilib.*, *194-197*, 501.

Blunt, M., Fayers, F. J., & Orr, F. M. (1993). Carbon dioxide in enhanced oil recovery, *En. Conv. Man.*, *34*, 1197.

Brennan, D. J., & Golonka, K. A. (2002). New factors for capital cost estimation in evolving process designs, *Chem. Eng. Res. & Des.*, *80*, 579.

Brønsted, J. N., & Koefoed, J. K. (1946). *Danske Vidensk. Selsk. (Mat. Fys. Skr.)*, *22*(17).

Brown, T. S., Kidnay, A. J., & Sloan, E. D. (1988). Vapor-liquid equilibria in the carbon dioxide - ethane system, *Fluid Phase Equilib.*, *40*, 169.

Buxton, A., Livingston, A. G., & Pistikopoulos, E. N. (1999). Optimal design of solvent blends for environmental impact minimization, *AIChE Journal*, *45*, 817.

Chapman, W. G., Gubbins, K. E., Jackson, G., & Radosz, M. (1989). SAFT: Equation-of-state solution model for associating fluids, *Fluid Phase Equilb.*, *52*, 31.

Chapman, W. G., Gubbins, K. E., Jackson, G., & Radosz, M. (1990). New reference equation of state for associating liquids, *Ind. Eng. Chem. Res.*, *29*, 1709.

Charoensombut-Amon, T., Martin, R. J., & Kobayashi, R. (1986). Application of a generalized multiproperty apparatus to measure phase equilibrium and vapor phase densities of supercritical carbon dioxide in n-hexadecane systems up to 26 MPa, *Fluid Phase Equilib.*, *31*, 89.

Chemmangattuvalappil, N. G., Eljack, F. T., Solvason, C. C., & Eden, M. R. (2009). A novel algorithm for molecular synthesis using enhanced property operators, *Comput. Chem. Eng.*, *33*, 636.

Chen, D., & Chen, W. (1992). *Huaxue Gongcheng*, *20*, 66.

Chou, G. F., Forbert, R. R., & Prausnitz, J. M. (1990). High-pressure vapor-liquid equilibria for carbon dioxide/n-decane, carbon dioxide/tetralin, and carbon dioxide/n-decane/tetralin at 71.1 and 104.4°C, *J. Chem. Eng. Data*, *35*, 26.

Cismondi, M., Diaz, M. S., Espinosa, S., & Brignole, E. A. (2003). Molecular solvent design and near critical solvents optimization with ECOFAC, *Latin American Applied Research*, *33*, 269.

Clark, G. N. I., Haslam, A. J., Galindo, A., & Jackson, G. (2006). Developing optimal Wertheim-like models of water for use in Statistical Associating Fluid Theory (SAFT) and related approaches, *Mol. Phys.*, *104*, 3561.

Davalos, J., Anderson, W. R., Phelps, R. E., & Kidnay, A. J. (1976). Liquid-vapor equilibria at 250.00 K for systems containing methane, ethane, and carbon dioxide, *J. Chem. Eng. Data*, *21*, 81.

Dohrn, R., & Pfohl, O. (2002). Thermophysical properties – industrial directions, *Fluid Phase Equilib.*, *194*, 15.

Donnelly, H. G., & Katz, D. L. (1954). Phase equilibria in the carbon dioxide-methane system, *Ind. Eng. Chem.*, *46*, 511.

dos Ramos, M. C., Blas, F. J., & Galindo, A. (2007). Modelling the phase equilibria and excess properties of the water + carbon dioxide binary mixture, *Fluid Phase Equilibria*, *261*, 359.

Douglas, J. (1988). *Conceptual Design of Chemical Processes*, McGraw-Hill, London.

Ducoulombier, D., Zhou, H., Boned, C., Peyrelasse, J., Saint-Guirons, H., & Xans, P. (1986). Pressure (1-1000 bars) and temperature (20-100°C) dependence of the viscosity of liquid hydrocarbons, *J. Phys. Chem.*, *90*, 1692.

Dunyushkin, I. I., Skripka, V. G., & Nenartovich, T. L. (1977). Phase equilibria in the systems CO_2 - n-butane - n-decane and CO_2 - methane - n-decane, *Deposited Doc. VINITI*, *2180-77*, 1.

Eden, M. R., Jørgensen, S. B., Gani, R., & El-Halwagi, M. M. (2004). A novel framework for simultaneous separation process and product design, *Chem. Eng. Process.*, *43*, 595.

Escobedo, J., & Mansoori, G. A. (1996). Surface tension prediction for pure fluids, *AIChE Journal*, *42*, 1425.

Filipe, E. J. M., de Azevedo, E. J. S. G., Martins, L. F. G., Soares, V. A. M., Calado, J. C. G., McCabe, C., & Jackson, G. (2000). Thermodynamics of liquid mixtures of xenon with alkanes:(xenon+ ethane) and (xenon+ propane), *J. Phys. Chem. B*, *104*, 1315.

Filipe, E. J. M., Martins, L. F. G., Calado, J. C. G., McCabe, C., & Jackson, G. (2000). Thermodynamics of liquid mixtures of xenon with alkanes:(xenon plus n-butane) and (xenon plus isobutane), *J. Phys. Chem. B*, *104*, 1322.

Fletcher, D. A., F., R., McMeeking, & Parkin, D. (1996). The United Kingdom Chemical Database Service, *J. Chem. Inf. Comput. Sci.*, *36*, 746.

Fredenslund, A., Jones, R. L., & Prausnitz, J. M. (1975). Group-contribution estimation of activity coefficients in nonideal liquid mixtures, *AIChE Journal*, *21*, 1086.

Fredenslund, A., & Mollerup, J. (1974). Measurement and prediction of equilibrium ratios for the C_2H_6+CO_2 system, *J. Chem. Soc. Faraday Trans. I*, *70*, 1653.

FT (2009). Financial Times Commodities. http://markets.ft.com/.

Galindo, A., & Blas, F. (2002). Theoretical examination of the global fluid phase behavior and critical phenomena in carbon dioxide + n-alkane binary mixtures, *J. Phys. Chem.*, *106*, 4503.

Galindo, A., Davies, L., Gil-Villegas, A., & Jackson, G. (1998). The thermodynamics of mixtures and the corresponding mixing rules in the SAFT-VR approach for potentials of variable range, *Mol. Phys.*, *93*, 241.

Galindo, A., Whitehead, P. J., Jackson, G., & Burgess, A. N. (1996). Predicting the high-pressure phase equilibria of water + n-alkanes using a simplified SAFT theory with transferable intermolecular interaction parameters, *J. Phys. Chem.*, *100*, 6781.

Gani, R., & Brignole, E. A. (1983). Molecular design of solvents for liquid extraction based on UNIFAC, *Fluid Phase Equilib.*, *13*, 331.

Gil-Villegas, A., Galindo, A., Whitehead, P. J., Mills, S. J., Jackson, G., & Burgess, A. N. (1997). Statistical associating fluid theory for chain molecules with attractive potentials of variable range, *J. Chem. Phys.*, *106*, 4168.

Giovanoglou, A., Barlatier, J., Adjiman, C. S., Pistikopoulos, E. N., & Cordiner, J. L. (2003). Optimal solvent design for batch separation based on economic performance, *AIChE Journal*, *49*, 3095.

Gros, H. P., Bottini, S. B., & Brignole, E. A. (1997). High pressure phase equilibrium modeling of mixtures containing associating compounds and gases, *Fluid Phase Equilib.*, *139*, 75.

Gross, J. (2005). An equation-of-state contribution for polar components: Quadrupolar molecules, *AIChE J.*, *51*, 2556.

Hamam, S., & Lu, B. (1974). Vapor-liquid equilibrium in the ethane - carbon dioxide system, *Can. J. Chem. Eng.*, *52*, 283.

Haslam, A. J., Galindo, A., & Jackson, G. (2008). Prediction of binary intermolecular potential parameters for use in modelling fluid mixtures, *Fluid Phase Equilib.*, *266*, 105.

Henni, A., Jaffer, S., & Mather, A. E. (1996). Solubility of N_2O and CO_2 in n-dodecane, *Can. J. Chem. Eng.*, *74*, 554.

Holderbaum, T., & Gmehling, J. (1991). PSRK – A group contribution equation of state based on UNIFAC, *Fluid Phase Equilib.*, *70*, 251.

Holmes, A. S., Ryan, J. M., Price, B. C., & Styring, R. E. (1982). Process improves acid gas separation, *Hydrocarbon Processing*, *61*, 131.

Hostrup, M., Harper, P. M., & Gani, R. (1999). Design of environmentally benign processes: integration of solvent design and separation process synthesis, *Comp. Chem. Eng.*, *23*, 1395.

Huron, M. J., & Vidal, J. (1979). New mixing rules in simple equations of state for representing vapour-liquid equilibria of strongly non-ideal mixtures, *Fluid Phase Equilib.*, *3*, 255.

Inomata, H., Tuchiya, K., Arai, K., & Saito, S. (1986). Measurement of vapor-liquid equilibria at elevated temperatures and pressures using a flow type apparatus, *J. Chem. Eng. Jpn.*, *19*, 386.

Iwai, Y., Hosotani, N., Morotomi, T., Koga, Y., & Arai, Y. (1994). High-pressure vapor-liquid equilibria for carbon dioxide + linalool, *J. Chem. Eng. Data*, *39*, 900.

Jackson, G., & Gubbins, K. E. (1989). Mixtures of associating spherical and chain molecules, *Pure & Appl. Chem.*, *61*, 1021.

Jennings, D. W., & Schucker, R. C. (1996). Comparison of high-pressure vapor-liquid equilibria of mixtures of CO_2 or propane with nonane and C_9 alkylbenzenes, *J. Chem. Eng. Data*, *41*, 831.

Kakalis, N. M. (2006). *Reliable and Efficient Use of the SAFT Equation of State in Process Modelling*, Ph.D. thesis, Imperial College London.

Kakalis, N. M. P., Kakhu, A. I., & Pantelides, C. C. (2004). Implementing SAFT-based thermodynamics in process modelling tools, in: *Proceedings of the 6th International Conference on Foundations of Computer-Aided Process Design*, p. 537, Michigan: CACHE Coporation.

Kaminishi, G., & Toriumi, T. (1968). Vapor-liquid equilibria in the systems: CO_2-CO, CO_2-CO-H_2 and CO_2-CH_4 (the co-operative researches on the fundamental studies of the liquid phase reactions at high pressures), *Rev. Phys. Chem. Japan*, *38*, 79.

Keshtkar, A., Jalali, F., & Moshfeghian, M. (1997). Evaluation of vapor-liquid equilibrium of CO_2 binary systems using UNIQUAC-based Huron-Vidal mixing rules, *Fluid Phase Equilib.*, *140*, 107.

Keskes, E. K. (2007). *Integrated Process and Solvent Design for CO_2 Removal from Natural Gas*, Ph.D. thesis, Imperial College London.

Klimeck, J., Kleinrahm, R., & Wagner, W. (2001). Measurements of the (p, ρ, T) relation of methane and carbon dioxide in the temperature range 240 K to 520 K at pressures up to 30 MPa using a new accurate single-sinker densimeter, *J. Chem. Therm.*, *33*, 251.

Kohl, A. L., & Nielsen, R. B. (1997). *Gas Purification*, 5th edition, Houston: Gulf.

Kohn, J. P., & Bradish, W. F. (1964). Multiphase and volumetric equilibria of the methane–n-octane system at temperatures between -110°C and 150°C, *J. Chem. Eng. Data*, *9*, 5.

Koonce, K. T., & Kobayashi, R. (1964). Vapor-liquid equilibrium coefficients determined by gas-liquid partition chromatography: Systems methane–propane–n-decane and methane–propane–n-heptane, *J. Chem. Eng. Data*, *9*, 494.

Lavender, H. M., Sage, B. H., & Lacey, W. N. (1940). Gas-liquid equilibrium constants: Methane - decane system, *Oil Gas J.*, *39*, 48.

Li, J. D., Fischer, K., & Gmehling, J. (1998). Prediction of vapor-liquid equilibria for asymmetric systems at low and high pressures with the PSRK model, *Fluid Phase Equilib.*, *143*, 71.

Lin, H. M., Sebastian, H. M., Simnick, J. J., & Chao, K. C. (1979). Gas-liquid equilibrium in binary mixtures of methane with n-decane, benzene, and toluene, *J. Chem. Eng. Data*, *24*, 146.

Lygeros, A. I., & Magoulas, K. G. (1986). Column flooding and entrainment. [Estimation of maximum allowable vapor velocity and entrainment in a distillation column], *Hydro. Proc.*, *65*, 43.

Lymperiadis, A., Adjiman, C. S., Galindo, A., & Jackson, G. (2007). A group contribution method for associating chain molecules based on the statistical associating fluid theory (SAFT-γ), *J. Chem. Phys*, *127*, 234903.

Lymperiadis, A., Adjiman, C. S., Jackson, G., & Galindo, A. (2008). A generalisation of the SAFT-γ group contribution method for groups comprising multiple spherical segments, *Fluid Phase Equilib.*, *274*, 85.

M. Glaser, M., Peters, C. J., van der Kool, H. H., & Lichtenthaler, R. N. (1985). Phase equilibria of (methane + n-hexadecane) and (p, v^m, T) of n-hexadecane, *J. Chem. Thermodyn.*, *17*, 803.

Macleod, D. B. (1923). On a relation between surface tension and density, *Trans. Faraday Soc.*, *19*, 38.

Marcoulaki, E. C., & Kokossis, A. C. (2000). On the development of novel chemicals using a systematic optimisation approach. Part II. Solvent design, *Chem. Eng. Sci.*, *55*, 2547.

McCabe, C., Galindo, A., Garcia-Lisbona, M. N., & Jackson, G. (2001). Examining the adsorption (vapor-liquid equilibria) of short-chain hydrocarbons in low-density polyethylene with the SAFT-VR approach, *Ind. Eng. Chem. Res.*, *40*, 3825.

McCabe, C., Galindo, A., Gil-Villegas, A., & Jackson, G. (1998a). Predicting the high-pressure phase equilibria of binary mixtures of n-alkanes using the SAFT-VR approach, *Int. J. Thermophys.*, *19*, 1511.

McCabe, C., Galindo, A., Gil-Villegas, A., & Jackson, G. (1998b). Predicting the high-pressure phase equilibria of binary mixtures of perfluoro-n-alkanes + n-alkanes using the SAFT-VR approach, *J. Phys. Chem. B*, *102*, 8060.

McCabe, C., Gil-Villegas, A., & Jackson, G. (1998). Predicting the high-pressure phase equilibria of methane+ n-hexane using the SAFT-VR approach, *J. Phys. Chem. B*, *102*, 4183.

McCabe, C., & Jackson, G. (1999). SAFT-VR modelling of the phase equilibrium of long-chain n-alkanes, *PCCP*, *1*, 2057.

Müller, E. A., & Gubbins, K. E. (2001). Molecular-based equations of state for associating fluids: A review of SAFT and related approaches, *Ind. Eng. Chem. Res.*, *40*, 2193.

Mohideen, M. J., Perkins, J. D., & Pistikopoulos, E. N. (1996). Optimal design of dynamic systems under uncertainty, *AIChE J.*, *42*, 2251.

Müller, D., & Marquardt, W. (1997). Dynamic multiple-phase flash simulation: Global stability analysis versus quick phase determination, *Comp. Chem. Eng.*, *21*, S817.

Nagahama, K., Konishi, H., Hoshino, D., & Hirata, M. (1974). Binary vapor-liquid equilibria of carbon dioxide - light hydrocarbons at low temperature, *J. Chem. Eng. Jpn.*, *7*, 323.

Nagarajan, N., & Robinson, R. L. (1986). Equilibrium phase compositions, phase densities, and interfacial tensions for CO_2+ hydrocarbon systems. 2. CO_2 + n-decane, *J. Chem. Eng. Data*, *31*, 168.

Newman, S. A. (1985). *Acid and Sour Gas Treating Processes*, Houston: Gulf.

Nguyen-Huynh, D., Tran, T. K. S., Tamouza, S., Passarello, J.-P., Tobaly, P., & de Hemptinne, J.-C. (2008). Modeling phase equilibria of asymmetric mixtures using a group-contribution SAFT (GC-SAFT) with a kij correlation method based on london's theory. 2. Application to binary mixtures containing aromatic hydrocarbons, n-alkanes, CO_2, N_2, and H_2S, *Ind. Eng. Chem. Res.*, *47*, 8859.

O'Connell, H. E. (1946). Plate efficiency of fractionating columns and absorbers, *Trans. Am. Inst. Chem. Eng.*, *42*, 741.

Odele, O., & Macchietto, S. (1993). Computer aided molecular design: A novel method for optimal solvent selection, *Fluid Phase Equilib.*, *82*, 47.

Ohgaki, K., & Katayama, T. (1977). Isothermal vapor-liquid equilibrium data for the ethane - carbon dioxide system at high pressures, *Fluid Phase Equilib.*, *1*, 27.

Orr, F. M., Johns, R. T., & Dindoruk, B. (1993). Development of miscibility in four-component CO_2 floods, *SPE Res. Eng.*, *8*, 135.

Orr, F. M., & Silva, M. K. (1983). Equilibrium phase compositions of CO_2/-hydrocarbon mixtures: Measurement by a continuous multiple contact experiment, *SPE Journal*, *23*, 272.

Papadopoulos, A. I., & Linke, P. (2006). Multiobjective molecular design for integrated process-solvent systems synthesis, *AIChE Journal*, *52*, 1057.

Papadopoulos, A. I., & Linke, P. (2008). Integrated solvent and process selection for separation and reactive separation systems, *Chem. Eng. Proc.*, *48*, 1047.

Paricaud, P., Galindo, A., & Jackson, G. (2002). Recent advances in the use of the SAFT approach in describing electrolytes, interfaces, liquid crystals and polymers, *Fluid Phase Equil.*, *194*, 87.

Paricaud, P., Galindo, A., & Jackson, G. (2004). Modeling the cloud curves and the solubility of gases in amorphous and semicrystalline polyethylene with the SAFT-VR approach and Flory theory of crystallization, *Ind. Eng. Chem. Res*, *43*, 6871.

Patel, B. H., Paricaud, P., Galindo, A., & Maitland, G. C. (2003). Prediction of the salting-out effect of strong electrolytes on water + alkane solutions, *Ind. Eng. Chem. Res.*, *42*, 3809.

Peng, D., & Robinson, D. (1976). A new two-constant equation of state, *Ind. Eng. Chem. Fundam.*, *15*, 59.

Peng, Y., Goff, K. D., dos Ramos, M. C., & McCabe, C. (2009). Developing a predictive group-contribution-based SAFT-VR equation of state, *Fluid Phase Equilib.*, *277*, 131.

Pereira, F. E., Keskes, E., Galindo, A., Jackson, G., & Adjiman, C. S. (2008). Chapter 8: Integrated design of CO_2 capture processes from natural gas,

in: Georgiadis, M., Pistikopoulos, E. N., & Kikkinides, E. S. (Eds.), *Energy Systems Engineering*, pp. 231–248, Weinheim: Wiley-VCH.

Pereira, F. E., Keskes, E., Galindo, A., Jackson, G., & Adjiman, C. S. (2010). *In preparation.*

Perry, R. H., Green, D. W., & Maloney, J. O. (1997). *Perry's Chemical Engineers' Handbook*, 7th edition, London: McGraw-Hill.

Peters, M. S., Timmerhaus, K. D., & West, R. E. (2002). *Plant design and economics for chemical engineers. 5th edition*, McGraw-Hill, London.

Pistikopoulos, E. N., & Stefanis, S. K. (1998). Optimal solvent design for environmental impact minimization, *Comp. Chem. Eng.*, *22*, 717.

Popov, V. N., & Sayapov, M. K. (1970). Density of carbon dioxide in the liquid phase, *Teploenergetika*, *4*, 76.

Process Systems Enterprise Ltd (2008). gPROMS Advanced User Guide.

Quayle, O. R. (1953). The parachors of organic compounds. An interpretation and catalogue, *Chem. Rev.*, *53*, 439.

Reamer, H. H., Olds, R. H., Sage, B. H., & Lacey, W. N. (1942). Phase equilibria in hydrocarbon systems. Methane - decane system, *Ind. Eng. Chem.*, *34*, 1526.

Reamer, H. H., Olds, R. H., Sage, B. H., & Lacey, W. N. (1944). Phase equilibria in hydrocarbon systems. Methane - carbon dioxide system in the gaseous region, *Ind. Eng. Chem.*, *36*, 88.

Reamer, H. H., & Sage, B. H. (1963). Phase equilibria in hydrocarbon systems. Volumetric and phase behavior of the n-decane-CO_2 system, *J. Chem. Eng. Data*, *8*, 508.

Renon, H., & Prausnitz, J. M. (1968). Local compositions in thermodynamic excess functions for liquid mixtures, *AIChE Journal*, *14*, 135.

Rowlinson, J. S., & Swinton, F. L. (1982). *Liquids and Liquid Mixtures*, 3rd edition, London: Butterworth.

Sebastian, H. M., Simnick, J. J., Lin, H. M., & Chao, K. C. (1980). Vapor-liquid equilibrium in binary mixtures of carbon dioxide + n-decane and carbon dioxide + n-hexadecane, *J. Chem. Eng. Data*, *25*, 138.

Shim, J., & Kohn, J. P. (1962). Multiphase and volumetric equilibria of the methane-n-hexane binary system at temperatures between -110° and 150°C, *J. Chem. Eng. Data*, *7*, 3.

Soave, G. (1972). Equilibrium constants from a modified Redlich-Kwong equation of state, *Chem. Eng. Sci.*, *27*, 1197.

Somait, F. A., & Kidnay, A. J. (1978). Liquid-vapor equilibria at 270.00 K for systems containing nitrogen, methane, and carbon dioxide, *J. Chem. Eng. Data*, *23*, 301.

Spee, M., & Schneider, G. M. (1991). Fluid phase equilibrium studies on binary and ternary mixtures of carbon dioxide with hexadecane, 1-dodecanol, 1,8-octanediol and dotriacontane at 393.2K and pressures up to 100MPa, *Fluid Phase Equilib.*, *65*, 263.

Srivastan, S., Darwish, N. A., Gasem, K. A. M., & Robinson, R. L. (1992). Solubility of methane in hexane, decane, and dodecane at temperatures from 311 to 423K and pressures to 10.4MPa, *J. Chem. Eng. Data*, *37*, 516.

Sultanov, R. G., Skripka, V. G., & Namiot, A. Y. (1971). Phase equilibria in the systems methane-n-hexadecane and nitrogen-n-hexadecane at high temperatures and pressures, *Deposited Doc. VINITI*, *2888-71*, 1.

Tamouza, S., Passarello, J.-P., Tobaly, P., & de Hemptinne, J.-C. (2004). Group contribution method with SAFT EOS applied to vapor liquid equilibria of various hydrocarbon series, *Fluid Phase Equilib.*, *222*, 67.

Tamouza, S., Passarello, J.-P., Tobaly, P., & de Hemptinne, J.-C. (2005). Application to binary mixtures of a group contribution SAFT EOS (GC-SAFT), *Fluid Phase Equilib.*, *228*, 409.

Tan, S. P., Adidharma, H., & Radosz, M. (2008). Recent advances and applications of statistical associating fluid theory, *Ind. Eng. Chem. Res.*, *47*, 8063.

Ulrich, G. D. (1984). *A guide to chemical engineering process design and economics*, New York: John Wiley and Sons.

Vargaftik, N. B. (1972). *Dictionary of Thermophysical Properties of Gases and Liquids*, Moskva.

Wagner, Z., & Wichterle, I. (1987). High-pressure vapour-liquid equilibrium in systems containing carbon dioxide, 1-hexene and n-hexane, *Fluid Phase Equilib.*, *33*, 109.

Wei, M., Brown, T., Kidnay, A., & Sloan, E. (1995). Vapor + liquid equilibria for the ternary system methane + ethane + carbon dioxide at 230K and its constituent binaries at temperatures from 207 to 270K, *J. Chem. Eng. Data*, *40*, 726.

Wei, Y. S., & Sadus, R. J. (2000). Equations of state for the calculation of fluid-phase equilibria, *AIChE Journal*, *46*, 169.

Wertheim, M. S. (1984a). Fluids with highly directional attractive forces. I. Statistical thermodynamics, *J. Stat. Phys.*, *35*, 19.

Wertheim, M. S. (1984b). Fluids with highly directional attractive forces. II. Thermodynamic perturbation theory and integral equations, *J. Stat. Phys.*, *35*, 35.

Wertheim, M. S. (1986a). Fluids with highly directional attractive forces. III. Multiple attraction sites, *J. Stat. Phys.*, *42*, 459.

Wertheim, M. S. (1986b). Fluids with highly directional attractive forces. IV. Equilibrium polymerization, *J. Stat. Phys.*, *42*, 477.

Wertheim, M. S. (1987). Thermodynamic perturbation theory of polymerization, *J. Chem. Phys.*, *87*, 7323.

Whitson, C. H., & Michelsen, M. L. (1989). The negative flash, *Fluid Phase Equilib.*, *53*, 51.

Wilson, G. M. (1964). Vapor-liquid equilibrium. XI. A new expression for the excess free energy of mixing, *J. Am. Chem. Soc.*, *86*, 127.

Xu, N., Dong, J., Wang, Y., & Shi, J. (1992a). *Huagong Xuebao*, *43*, 640.

Xu, N., Dong, J., Wang, Y., & Shi, J. (1992b). High pressure vapor liquid equilibria at 293K for systems containing nitrogen, methane and carbon dioxide, *Fluid Phase Equilib.*, *81*, 175.

A Economic models

A.1 Total capital investment, TCI

A.1.1 Purchase cost

The calculation of the purchased costs for all units in USD (1991 basis) are presented in this section, assuming carbon steel (CS) is used.

Pump The cost of the pump is a function of the consumed power of the pump, W_{pump} (in kW). Assuming an overall efficiency factor of 90%, the consumed power is then $W_{pump}/0.9$. The purchased cost of the pump is given by Perry, Green & Maloney (1997) (Chap 9 - page 69). Two exponential laws are given for two operating ranges. For a small pump (with a power below 30 kW), the purchased cost exponential law is:

$$\text{Purchased Cost} = \frac{931}{1000} \times 1600 \times (\frac{W_{pump}/0.9}{7.5})^{0.3} = 840.{W_{pump}}^{0.3} \quad (24)$$

For a large pump, for which $W_{pump}/0.9 > 30$:

$$\text{Purchased Cost} = \frac{931}{1000} \times 4400 \times (\frac{W_{pump}/0.9}{74.6})^{0.67} = 244.53.{W_{pump}}^{0.67} \quad (25)$$

Flash drum: To determine the cost of the flash drum, the volume of the drum or pressure vessel, V_{vessel} (in m^3), is needed. This is based on how much time the liquid remains in the tank. The longer the liquid remains in the tank, the less gas will remain trapped in the liquid. A residence time τ of 5 minutes (300 sec) is considered satisfactory to achieve a good separation for oil with a medium viscosity (API, 1989). If we assume that equal volumes of liquid and vapour are present in the tank at any time, then we can deduce from the liquid molar flowrate F_{liquid} (in $mol.s^{-1}$) what the volume of the pressure vessel V_{vessel} is:

$$V_{vessel} = 2F_{liquid}\tau V_{liquid}, \tag{26}$$

where V_{liquid} is the molar volume of the liquid in $m^3.mol^{-1}$.

The purchase cost of the pressure vessel has been given by Douglas (1988) as a function of the diameter and height of the tank and can be re-arranged as a function of V_{vessel} only (in m^3) assuming an aspect ratio of 4. The pressure of the vessel also has a strong impact on its cost, as an increased thickness is required when the pressure increases. In expression (26), the cost was calculated for a pressure vessel withstanding atmospheric pressure. A factor F_p must be applied to the cost to account for higher pressures. This gives the following equation:

$$\mathrm{PC}_{1991,CS}(\text{vessel}) = 4832.42F_pV_{vessel}^{0.6287}. \tag{27}$$

A second-order approximation of the pressure factor is used:

$$F_p = 0.057375.P_{vessel}^2 + 0.05805.P_{vessel} + 1.0136, \tag{28}$$

where P_{vessel} is the pressure of the vessel in MPa.

Distillation Column Trays and Tower Internals:

Sizing: Number of trays Each tray has been considered as ideal, i.e., complete mixing and thermodynamic equilibrium have been assumed. To take into account the non-ideality of the absorption, an efficiency factor is used. One

way of doing this is to use an overall tray efficiency factor E_0, which is defined as follows:

$$E_0 = N_{theoretical}/N_{actual}. \tag{29}$$

O'Connell (1946) has shown a strong correlation between an overall tray efficiency factor and some properties of the liquid. We have developed an alternative correlation for the experimental data used by O'Connell:

$$E_0 = 0.5 + 0.5 \tanh\left(0.5738 \log \frac{\rho_L}{m M_L \mu_{L,N_a}} - 0.2585\right), \tag{30}$$

where $m = y_{CO_2}/x_{CO_2}$ is the ratio of the mole fraction of CO_2 in the gas feed to the mole fraction of CO_2 in the liquid, M_L is the liquid molecular weight, μ_L is the liquid viscosity (in cP), and ρ_L is the liquid density (in lb/ft^3).

To calculate μ_L and ρ_L, we assume that the liquid consists only of n-alkane, so the viscosity and the density are only functions of P and T, the average pressure and temperature, and the alkane number N_a. A correlation has been proposed by Ducoulombier, Zhou, Boned, Peyrelasse, Saint-Guirons *et al.* (1986), who gives the dynamic viscosities μ_{N_a} (in cP) of n-alkanes (from n-decane to n-octadecane) as a function of pressure (1-1000 bar) and temperature (20-100°C) as

$$\mu_L = \mu_{L,N_a} = \mu_{N_{14}} \cdot \left(\frac{T_{c,N_a}}{T_{c,N_{14}}}\right)^{\cdot} \left(\frac{P_{c,N_a}}{P_{c,N_{14}}}\right)^{B} \left(\frac{MW_a}{MW_{14}}\right)^{C}, \tag{31}$$

where $A = 1.385374$, $B = -0.756972$ and $C = -0.532041$, T_{c,N_a} is the critical temperature of n-alkane a in degrees Celsius, P_{c,N_a} its critical pressure in bars, MW_a its molecular weight in grams, and $\mu_{N_{14}}$ is the viscosity of n-tetradecane given by:

$$\mu_{N_{14}} = \exp\left(aP^2 + bP + c + \frac{dP^4 + eP^3 + fP^2 + gP + h}{T - iP^2 - jP - k}\right), \tag{32}$$

where P is the pressure in bar, and T the temperature in degrees Celsius, and the values of the constants are: $a = -4.868729.10^{-6}$, $b = 6.162691.10^{-3}$, $c = -3.461585$, $d = 1.545022.10^{-9}$, $e = -3.443880.10^{-6}$, $f = 4.187426.10^{-3}$, $g = -2.527380$, $h = 874.0397$, $i = -2.985316.10^{-4}$, $j = 0.3435125$, and $k = -182.6151$.

The critical pressure and temperature of the entire n-alkane family are required to apply this equation. For simplicity, we have produced a correlation for the critical pressure and temperature of the n-alkane family (from ethane to eicosane). The critical temperature in K is given as a function of the number of carbon atoms, N_a, with an average percentage error of around 1%, as:

$$T_{c,N_a} = 855 - 10^{(-0.043170N_a + 2.809056)}, \tag{33}$$

and the critical pressure is given in MPa as a function of the critical temperature, with an average percentage error around 4%, by:

$$P_{c,N_a} = 7.11345 - 0.007919T_{c,N_a}. \tag{34}$$

Sizing: Tray stack height and column height The tray stack height h is deduced from the actual number of trays N_{actual}, provided that a tray spacing TS has been chosen. This is generally taken as 24 inches, i.e., $TS = 0.6096$ m. Some additional space at the top and at the bottom of the column is required for the flow, which is approximately 15% of the tray stack height, so that the column height H in m is:

$$H = 1.15N_{actual}TS = 1.15\frac{N_{theoretical}}{E_0}TS. \tag{35}$$

The tray stack height h in m is

$$h = N_{actual}TS. \tag{36}$$

Sizing: Column Diameter The choice of column diameter is crucial to ensure stable operation within the column. Indeed, the counter-current flow of the solvent and the gas can generate numerous flow patterns, depending on the gas and liquid flows. Perry, Green & Maloney (1997) lists a number of problems that can occur such as entrainment flooding, entrainment, weeping and downcomer flooding.

An appropriate column diameter can be chosen based on the minimum velocity at which entrainment flooding occurs, $U_{n,flood}$ (m.s^{-1}), as explained by

Douglas (1988) and Perry, Green & Maloney (1997). Normal operation requires a flowrate of about 80% of the maximum:

$$U_n = 0.8U_{n,flood}, \tag{37}$$

where U_n is the gas velocity (in m.s^{-1}) through the net column area A_n (in m^2).

$U_{n,flood}$ is obtained from the force balance between the droplet weight and the drag force exerted by the gas stream as

$$U_{n,flood} = C_{sb,flood}.\left(\frac{\sigma_L}{20}\right)^{0.2}.\sqrt{\frac{\rho_L - \rho_V}{\rho_V}}, \tag{38}$$

where σ_L is the liquid surface tension (in mN.m^{-1}), ρ_L is the liquid density in kg.m^{-3}, and ρ_V is the gas density in kg.m^{-3}. $C_{sb,flood}$ is obtained from a correlation established by Lygeros & Magoulas (1986), and is expressed as a function of the tray spacing TS (in inches) and a ratio of liquid to vapour kinetic energy through F_{LV}:

$$C_{sb,flood} = 0.0105 + 8.127 \times 10^{-4}(25.4TS)^{0.755} \exp\left(-1.463.{F_{LV}}^{0.842}\right), \tag{39}$$

where $C_{sb,flood}$ has the units m.s^{-1}, and F_{LV} is dimensionless. The ratio of liquid to vapour kinetic energy through F_{LV} is defined as follows:

$$F_{LV} = \sqrt{\frac{\rho_L}{\rho_V}}.\frac{q_L}{q_V}. \tag{40}$$

An estimate of the liquid surface tension is required in equation (38). It can be obtained through the liquid and gas densities from the parachor correlation of Macleod (1923):

$$P_\rho = \sigma_L^{1/4}\frac{M_L}{(\rho_L - \rho_V)}, \tag{41}$$

where M_L is the liquid molecular weight (in g.mol^{-1}), ρ_L and ρ_V are the liquid and vapour densities (in kg.m^{-3}), σ_L the vapour-liquid surface tension (in mN.m^{-1}), and P_ρ a constant independent of temperature called the parachor. Quayle (1953) used experimental surface tension and density data for numerous compounds to calculate the P_ρ constants of hydrocarbons. A full review of the

subject is given by Escobedo & Mansoori (1996). We apply the Macleod correlation to a multi-component mixture, as we need a rough estimate of the surface tension. A correlation can be established based on the available experimental data, where the parachor P_ρ is given as a function of the number of carbon atoms N_a of the alkane by

$$P_\rho = 39.91 N_a + 31.67. \tag{42}$$

The net area of the column A_n(in m^3) is related to the gas velocity via

$$A_n = q_V / U_n, \tag{43}$$

where q_V is the volumetric gas flow rate (in $\mathrm{m}^3.\mathrm{s}^{-1}$) and A_n is the net area. One part of the total cross section of the column A_t is occupied by the downcomers; it is usually equivalent to 20% of the net area A_n so that

$$A_t = 1.2 A_n. \tag{44}$$

The column diameter (in m) can then easily be calculated as

$$D = 2\sqrt{A_t/\pi}. \tag{45}$$

Costing of absorber The cost of the absorber (in \$) is split between the cost of the shell and of the trays. Correlations have been given by Douglas (1988). The cost of the shell is obtained as for a pressure vessel:

$$\mathrm{PC}_{1991,CS}(\text{shell}) = 3185 F_p D^{1.066} H^{0.82}, \tag{46}$$

where D is the column diameter in m, H is the column height in m, and F_p is the pressure factor. The cost of the trays is a function of the tray stack height h (in m), the diameter D (in m), and factor F_c:

$$\mathrm{PC}_{1991,CS}(\text{trays}) = 323.3 D^{1.55} h F_c. \tag{47}$$

The F_c factor accounts for three characteristics of the trays: the spacing, the tray type, and the material. This is done via other factors: F_s is for the tray

spacing, F_t for the tray type, and F_m for the tray material. The values of the factors are shown in table 4.

The F_c factor is then the sum of the other three factors: $F_c = F_s + F_t + F_m$. In our current work, we choose plate trays made of carbon steel with a tray spacing of 24 in. Hence, the F_c factor is 1.

The absorber purchase cost is then

$$\mathrm{PC}_{1991,CS}(\text{absorber}) = \mathrm{PC}_{1991,CS}(\text{shell}) + \mathrm{PC}_{1991,CS}(\text{trays}). \tag{48}$$

A.1.2 From purchase cost to on-site direct cost

The purchase cost of each unit (1991 USD basis) has been obtained for carbon steel material (CS). In order to account for the price of the actual material Mat, a material factor f_m should be applied to $PC_{1991,CS}(i)$ as shown below:

$$PC_{1991,Mat}(i) = PC_{1991,CS}(i) f_m, \tag{49}$$

where subscript i denotes the unit (flash drum, pump or absorber). In this work, f_m is taken equal to 1. An overall installation factor, $OIF(i)$, is applied to obtain the installation cost, IC_{1991}. The factor is applied to the purchased cost of item i made of carbon steel, so that

$$IC_{1991}(i) = PC_{1991,CS}(i) OIF(i). \tag{50}$$

The installation costs are independent of the material of the equipment. A first-order approximation of OIF has been obtained from the data in Brennan & Golonka (2002), giving

$$OIF(i) = \max\left(a(i) \log(PC_{1991,CS}(i)) + b(i), c(i)\right), \tag{51}$$

where the coefficients $a(i)$, $b(i)$ and $c(i)$ are given in table 5.

The direct cost of item i in USD 1991, $DC_{1991}(i)$, is the sum of the purchased cost and the installation cost:

$$DC_{1991}(i) = PC_{1991,Mat}(i) + IC_{1991}(i). \tag{52}$$

The direct cost of item i is updated to a 2008 level. The update factor is the Marshall & Swift index:

$$DC_{2008}(i) = \frac{M\&S_{2008}}{M\&S_{1991}} DC_{1991}(i), \tag{53}$$

where $M\&S_{2008} = 1431.7$ and $M\&S_{1991} = 931$.

The total on-site direct cost of the plant, DC_{2008}, is the sum of the individual direct cost of each equipment:

$$DC_{2008} = \sum_i DC_{2008}(i) \tag{54}$$

A.1.3 From on-site direct cost to total capital investment

The total on-site direct cost of the plant is a fraction of the total capital investment. Numerous other costs have to be accounted for such as off-site direct costs (buildings, yard improvement, service facilities, nonprocess equipment), indirect costs (engineering and supervision, construction expenses, contractor's fee, and contingency), working capital (raw material, accounts receivable, cash in hand, accounts payable, and taxes payable) and start-up costs (process modifications, start-up labour, and loss in production). A breakdown is proposed by Douglas (1988). The total capital cost breakdown is given in table 6. The capital breakdown is given as a percentage of the total fixed capital investment (FCI) or of the total capital investment (TCI). Average figures have been chosen for this study. By adding all the contributions, we find the following relation:

$$\text{TCI} = \frac{130}{55} DC_{2008}. \tag{55}$$

A.2 Total operating cost, TOC

Operating cost for a separation process such as the CO_2/CH_4 absorption process includes personnel cost (labour and supervision) to operate the plant, utilities, and the cost of raw materials. Indirect expenses must also to be included, such as depreciation of materials, equipment and building, as well as taxes, insurance, maintenance, royalties, and non-manufacturing costs such as administration and R&D costs. Total Operating Costs are divided into three parts:

- Direct Operating Costs
- Fixed Charges
- Plant Overhead

A.2.1 Direct Operating Costs

Utilities & raw materials costs Several utilities are used in the process such as a solvent, electricity, steam or some cooling water. The solvent is an n-alkane hence a good approximation of its cost is to take the price of a barrel of oil. This fluctuates significantly and we assume here 75 USD on a 2004-2008 basis. Solvent costs are likely to be small. The cost of the solvent is given in USD.mol^{-1}:

$$\text{Solvent Cost, in 2008 USD.mol}^{-1} = 314.5 \times 10^{-6}. \tag{56}$$

The electricity cost is given by Peters, Timmerhaus & West (2002) for the year 2000 as 0.045 USD/kWh. This cost should be updated for year 2008, and is given in USD/kWh:

$$\text{Electricity Cost, in 2008 USD/kWh} = 0.045 \times \frac{M\&S_{2008}}{M\&S_{2000}} \tag{57}$$

Where $M\&S_{2000} = 1089$. Steam is assumed to be available from a unit which is already in place near the plant, so only the operating cost has to be considered. According to Perry's handbook (Perry, Green & Maloney, 1997), Chap 9, page 75), the cost for generating steam depends on the steam pressure. It ranges from 7.90 to 9.50 USD/ton at 3550 kPa; 3.70 to 7.70 USD/ton at 790 kPa; and 2.00 to 3.70 USD/ton for exhaust steam. These costs have been given for a Marshall and Swift index of 1000, and hence need to be updated to today's price. For our study, we have produced a linear correlation between the steam temperature T_{steam} and the cost as shown below:

$$\text{Steam Cost, in 2008 USD/ton} = \frac{M\&S_{2008}}{1000}.(0.0411.T_{steam} - 12.478). \tag{58}$$

The cooling water price is given by Peters, Timmerhaus & West (2002) for the year 2000 as 0.03 USD/1000gal. This cost should also be updated for the year 2008, and is given in USD.mol^{-1} as

$$\text{Cooling Cost, in 2008 USD.mol}^{-1} = 0.03 \times 2.6417.10^{-4} \times 18 \times \frac{M\&S_{2008}}{M\&S_{2000}}. \quad (59)$$

Operating labour costs The operating labour cost varies depending on the equipment. Only the absorber is considered to require labour. It is assumed that 0.35 of a worker is needed to operate the process. This implies that the process is co-located with other processes which can make use of the remaining hours of the worker employed. The US average labour cost was 25.58 USD.(worker.hr)$^{-1}$ for 2001 for common labour, according to Peters, Timmerhaus & West (2002). This cost has been updated to 2008 USD:

$$\text{Operating Labour Cost, in 2008-USD/year} = \frac{M\&S_{2008}}{M\&S_{2001}} \times 25.58 \times N \quad (60)$$

Other direct operating cost The other direct operating costs accounted for in our study are listed below (estimates have been taken from Douglas (1988):

- Maintenance & Repairs $\simeq$ 4% of Fixed-capital investment (FCI)
- Operating Supplies $\simeq$ 15% of Maintenance & Repairs
- Direct Supervision and Clerical Labour $\simeq$ 20% of Operating Labour
- Laboratory Charges $\simeq$ 15% of Operating Labour
- Patents and Royalties have been neglected.

A.2.2 Fixed charges

Based on Douglas (1988), fixed charges of 3% of the total capital investment are applied to take local taxes and insurance into account.

A.2.3 Plant overhead

According to Douglas (1988), plant overheads represent about 50-70% of the cost for operating labour, supervision, and maintenance. For this study, we use the following expression:

$$\text{Plant Overheads} = 0.6(\text{Maintenance \& Repairs} + \text{Operating Labour} + \text{Supervision}). \tag{61}$$

A.3 Revenue

The price of the sale gas can be estimated based on a typical price in 2004-2008 of 6 USD/million BTU. This base price can be used to estimate the revenues produced by the sale of the natural gas production over the life of the plant. We assume that the production of natural gas will last n_{year} years and remain constant in quantity and composition. The annual revenue from the natural gas sales NGS (in Million USD/year) is calculated as follows:

$$NGS = 0.151865 F_{clean-NG}, \tag{62}$$

where $F_{clean-NG}$ is the molar flowrate of sale gas in mol.s^{-1}. It is expected that the sale price of natural gas will increase with time as well as the Marshall & Swift index. Uncertainties on the natural gas price are high. For this reason, we adopt a conservative approach, where the revenue as well as the operating cost remain constant for the duration of the project. As a result, the present value of the natural gas sales $PV_{gas-sales}$ is given by:

$$PV_{gas-sales} = NGS \times n_{year}, \tag{63}$$

where n_{year} is the life of the plant in years ($n_{year} = 15$ is assumed).

List of Tables

1 SAFT-VR parameters for CH_4 and CO_2, where m_i corresponds to the number of spherical segments in the model chain, σ_{ii} to the hard-core diameter of the segments, and ϵ_{ii}/k_B and λ_{ii} to the square-well depth and range, respectively. The parameters are given as scaled to the critical pressure and temperature for each pure component; the corresponding unscaled parameters are also reported. 61

2 Results of the binary interaction parameter estimation: k_{ij}^{ϵ} is the binary interaction parameter for the unlike attractive interaction, T range is the temperature range of the experimental data used, N_{exp} is the total number of experimental data points included in the estimation, %ADD P and AAD y are the average deviations as defined in equations (9) and (10), respectively. 62

3 Results of the optimisations for different optimisation variables, equipment sizes, operating costs, revenue and net present value (NPV) of the process after 15 years. 63

4 Cost factors for the different tray type, spacing, and materials. . 64

5 OIF: Overall installation cost factors coefficients used in this work. 65

6 Breakdown of the total capital investment. 66

Table 1: SAFT-VR parameters for CH_4 and CO_2, where m_i corresponds to the number of spherical segments in the model chain, σ_{ii} to the hard-core diameter of the segments, and ϵ_{ii}/k_B and λ_{ii} to the square-well depth and range, respectively. The parameters are given as scaled to the critical pressure and temperature for each pure component; the corresponding unscaled parameters are also reported.

Component $\boldsymbol{i}$	$\boldsymbol{m_i}$	$\boldsymbol{\sigma_{ii}}$(Å)	$\boldsymbol{\epsilon_{ii}/k_B}$(K)	$\boldsymbol{\lambda_{ii}}$
$\mathbf{CH_4}$	1	4.0576	156.50	1.4479
$\mathbf{CH_4}$ (unscaled)	1	3.6847	167.30	1.4479
$\mathbf{CO_2}$	2	3.1364	168.89	1.5157
$\mathbf{CO_2}$ (unscaled)	2	2.7864	179.27	1.5157

Table 2: Results of the binary interaction parameter estimation: k_{ij}^{ϵ} is the binary interaction parameter for the unlike attractive interaction, T range is the temperature range of the experimental data used, N_{exp} is the total number of experimental data points included in the estimation, %ADD P and AAD y are the average deviations as defined in equations (9) and (10), respectively.

Mixture i + j	k_{ij}^{ϵ}	T range [K]	N_{exp}	%AAD P	AAD y
CH_4+CO_2	+0.036798	199.82-301.00	317	2.1	0.0236
C_{10}+CH_4	-0.053006	244.26-477.59	111	7.6	0.0027
C_{10}+CO_2	+0.089642	277.59-477.59	85	9.9	0.0010

Table 3: Results of the optimisations for different optimisation variables, equipment sizes, operating costs, revenue and net present value (NPV) of the process after 15 years.

% CO_2 in inlet stream	10.0	30.0	70.0
Solvent flowrate 100*mol.s^{-1}	17.8	16.4	4.6
n-alkane, N_a	12.5	12.4	9.3
Absorber pressure MPa	3.0	4.1	7.9
Column height (m)	50.0	44.0	37.3
Column cross section (m^2)	20.5	15.3	5.6
Tank volume (m^3)	255.0	232.2	46.5
Temperature absorber top (K)	303.3	301.7	236.2
Temperature absorber bottom (K)	305.1	307.1	292.9
% CH_4 recovery	68.0	54.4	42.6
% CO_2 in outlet waste stream	22.0	47.5	80.2
TCI mUSD	71.8	55.8	31.1
TOC mUSD	100.0	86.2	45.7
Revenue gas sales mUSD	1513.3	941.7	315.9
Predicted NPV mUSD	1341.5	799.7	239.1

Table 4: Cost factors for the different tray type, spacing, and materials.

Tray spacing in in.	24	18	12
F_s	1.0	1.4	2.2
Tray type	Plate	Sieve	Bubble cap
F_t	0.0	0.0	1.8
Tray material	carbon steel CS	stainless steel SS	Monel
F_m	0.0	1.7	8.9

Table 5: OIF: Overall installation cost factors coefficients used in this work.

Equipment	$a(i)$	$b(i)$	$c(i)$
Pump	-2.339	8.1246	2.23
Flash drum	-2.3595	8.0785	2.15
Absorber	-4.2401	13.76	2.96

Table 6: Breakdown of the total capital investment.

Breakdown	This study	Recommended by Douglas (1988)
Total Capital Investment (TCI)	130	TCI = A + B + C
A. Fixed Capital Investment (FCI)	100	
1/ Direct Cost	75	70-85% of FCI
a/ Onsite Cost	55	50-60% of FCI
b/ Offsite Cost	20	-
2/ Indirect Cost	25	15-30% of FCI
a/ Engineering & Supervision	-	4-21% of FCI
b/ Construction Expenses	-	4.8-22% of FCI
c/ Contractor's fee	-	1.5-5% of FCI
d/ Contingency	-	5-20% of FCI
B. Working Capital	20	10-20% of TCI
C. Start-up	10	8-10% of FCI

List of Figures

1 A basic process flowsheet for the separation of CO_2 and CH_4 through physical absorption into an n-alkane solvent. 70

2 Pressure-volume isotherms for CH_4. The isotherms calculated with SAFT-VR (continuous curves) are compared with experimental data in the vapour-liquid coexistence (empty squares) (Vargaftik, 1972) and supercritical (filled circles) regions (Klimeck, Kleinrahm & Wagner, 2001). 71

3 Pressure-volume isotherms for CO_2. The isotherms calculated with SAFT-VR (continuous curves) are compared with experimental data in the vapour-liquid coexistence (empty squares) (Vargaftik, 1972), supercritical (filled triangles) (Reamer, Olds, Sage & Lacey, 1944), and subcritical (filled squares) (Popov & Sayapov, 1970) regions. 72

4 Pressure-composition representation of the vapour-liquid equilibria for different temperatures for the CH_4 + CO_2 mixtures. The description obtained with the SAFT-VR equation of state (continuous curves) is compared with experimental data (filled diamonds) (Donnelly & Katz, 1954). 73

5 Pressure-composition representation of the vapour-liquid equilibria of the mixture CH_4 + C_{10} (n-decane) for temperatures 310.93K, 344.26K and 377.59K (from top to bottom). The description obtained with the SAFT-VR equation of state (continuous curves) is compared with experimental data (filled circles) (Reamer, Olds, Sage & Lacey, 1942). 74

6 Pressure-composition representation of the vapour-liquid equilibria of the mixture CO_2 + C_{10} (n-decane) for temperatures 310.93K, 344.26K and 377.59K (from top to bottom). The description obtained with the SAFT-VR equation of state (continuous curves) is compared with experimental data (filled circles) (Reamer & Sage, 1963). 75

7 Pressure-composition representation of the vapour-liquid equilibria of the mixture CH_4 + C_{16} (n-hexadecane) for temperatures 373.15K, 423.15K and 473.15K (from top to bottom). The predictions obtained with the SAFT-VR equation of state (continuous curves) are compared with experimental data (filled circles) (Sultanov, Skripka & Namiot, 1971) 76

8 Pressure-composition representation of the vapour-liquid equilibria of the mixture of CO_2 + C_{16} (n-hexadecane) for temperatures 323.15K, 343.15K and 393.20K (from top to bottom). The predictions obtained with the SAFT-VR equation of state (continuous curves) are compared with experimental data (Charoensombut-Amon, Martin & Kobayashi, 1986) for T = 323.15K and 343.15K; (Spee & Schneider, 1991) for T = 393.20K) 77

9 Pressure-composition representation of the vapour-liquid equilibria of the mixture CO_2 + n-alkane for a fixed temperature 313.15K (from top to bottom, n-alkanes are n-hexane C_6, n-octane C_8, n-dodecane C_{12} and n-hexadecane C_{16}). The predictions obtained with the SAFT-VR equation of state (continuous curves) are compared with experimental data (filled circles (Wagner & Wichterle, 1987) for n-hexane; (Chen & Chen, 1992) for n-octane, (Henni, Jaffer & Mather, 1996) for n-dodecane and (Charoensombut-Amon, Martin & Kobayashi, 1986) for n-hexadecane). 78

10 Pressure-composition representation of the vapour-liquid equilibria for the mixture CH_4 + n-alkane for a fixed temperature 323.15K (from top to bottom, n-alkanes are n-hexane C_6, n-octane C_8, n-decane C_{10}, n-dodecane C_{12} and n-hexadecane C_{16} (T=320K for C_{16})). The predictions obtained with the SAFT-VR equation of state (continuous curves) are compared with experimental data (filled circles (Shim & Kohn, 1962) for n-hexane; (Kohn & Bradish, 1964) for n-octane; (Beaudoin & Kohn, 1967) for n-decane; (Srivastan, Darwish, Gasem & Robinson, 1992) for n-dodecane and (M. Glaser, Peters, van der Kool & Lichtenthaler, 1985) for n-hexadecane) 79

11 Vapour-liquid equilibrium of the ternary mixture: CO_2 + CH_4 + C_{10} (n-decane). Three data sets obtained at different pressures of 4.9 MPa, 9.8 MPa, 14.7 MPa, and 19.6 MPa, and a temperature of 344.15 K, are shown. The experimental points are shown as diamonds (joined by tie lines, (Dunyushkin, Skripka & Nenartovich, 1977)) and the SAFT-VR calculations as the continuous curves. 80

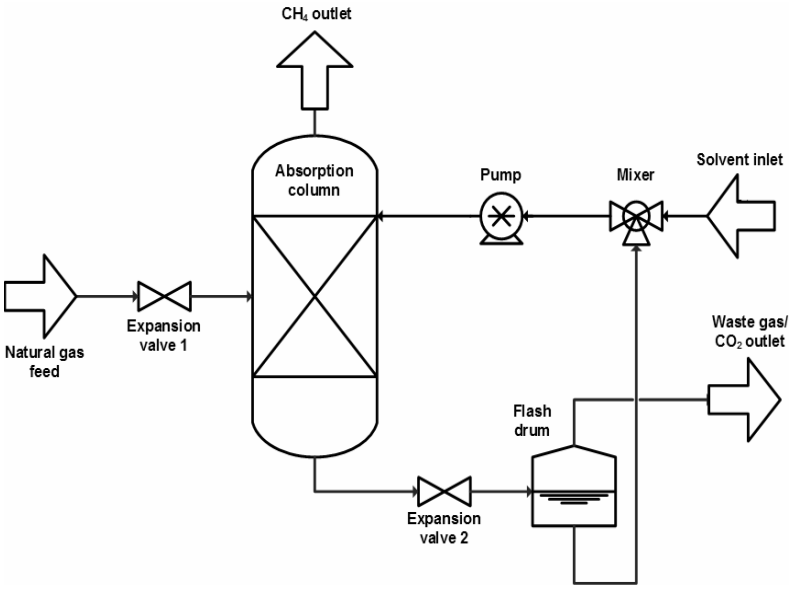

Figure 1: A basic process flowsheet for the separation of CO_2 and CH_4 through physical absorption into an n-alkane solvent.

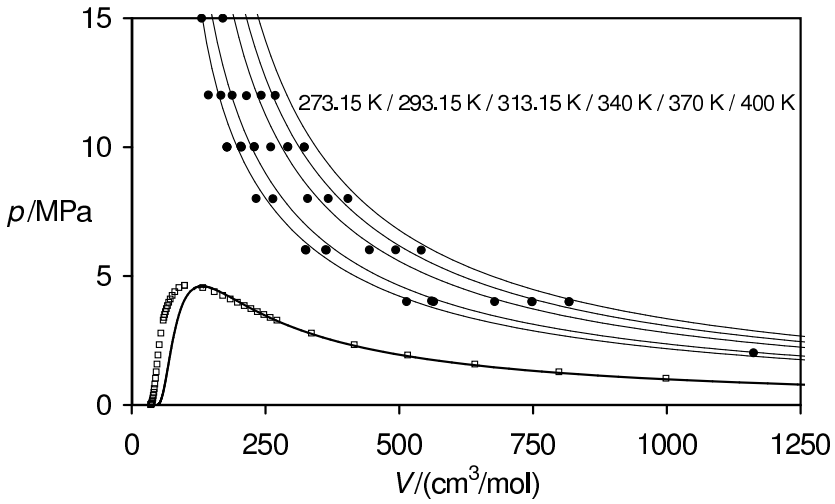

Figure 2: Pressure-volume isotherms for CH_4. The isotherms calculated with SAFT-VR (continuous curves) are compared with experimental data in the vapour-liquid coexistence (empty squares) (Vargaftik, 1972) and supercritical (filled circles) regions (Klimeck, Kleinrahm & Wagner, 2001).

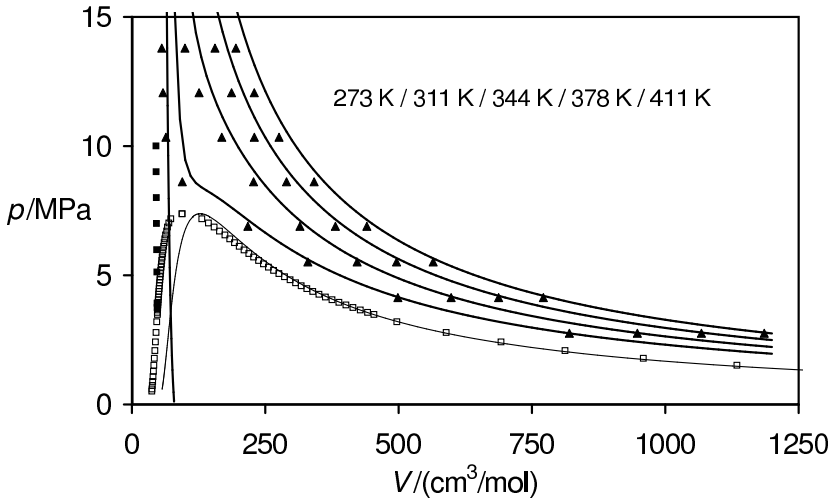

Figure 3: Pressure-volume isotherms for CO_2. The isotherms calculated with SAFT-VR (continuous curves) are compared with experimental data in the vapour-liquid coexistence (empty squares) (Vargaftik, 1972), supercritical (filled triangles) (Reamer, Olds, Sage & Lacey, 1944), and subcritical (filled squares) (Popov & Sayapov, 1970) regions.

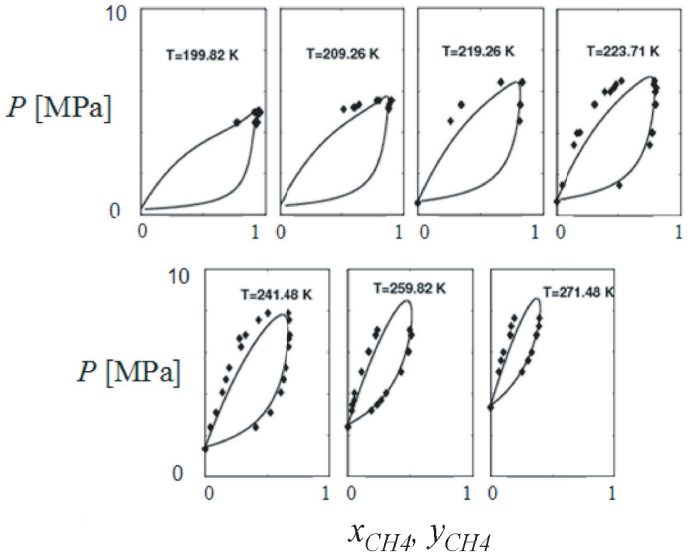

Figure 4: Pressure-composition representation of the vapour-liquid equilibria for different temperatures for the CH_4 + CO_2 mixtures. The description obtained with the SAFT-VR equation of state (continuous curves) is compared with experimental data (filled diamonds) (Donnelly & Katz, 1954).

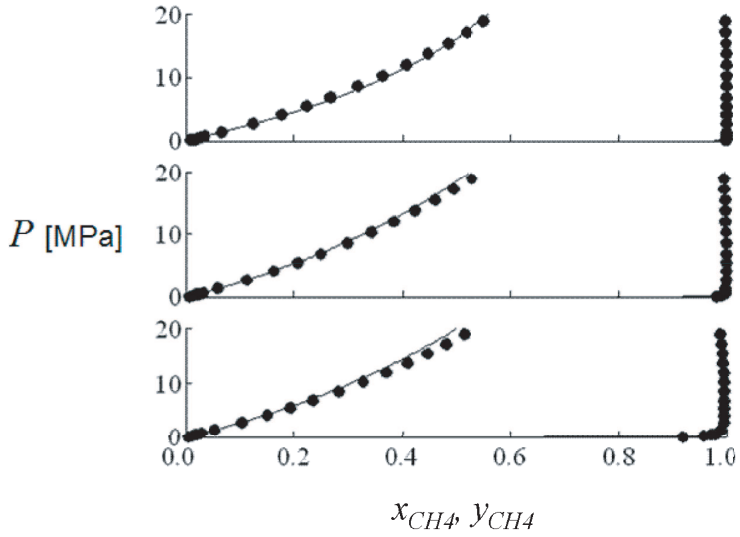

Figure 5: Pressure-composition representation of the vapour-liquid equilibria of the mixture CH_4 + C_{10} (*n*-decane) for temperatures 310.93K, 344.26K and 377.59K (from top to bottom). The description obtained with the SAFT-VR equation of state (continuous curves) is compared with experimental data (filled circles) (Reamer, Olds, Sage & Lacey, 1942).

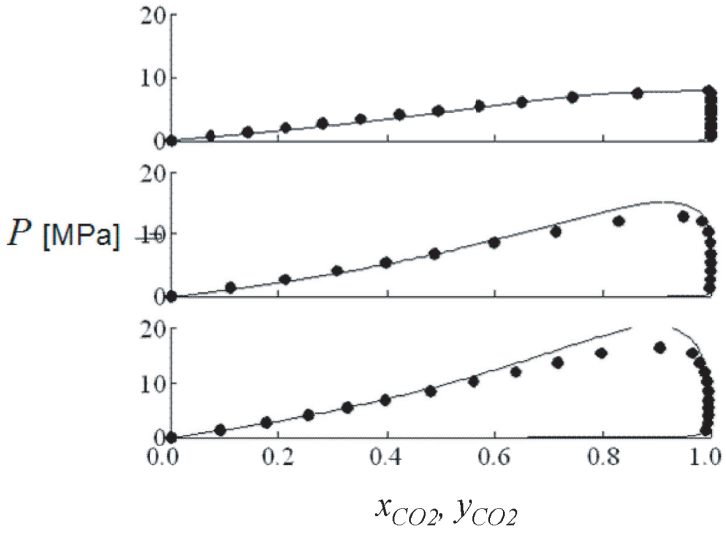

Figure 6: Pressure-composition representation of the vapour-liquid equilibria of the mixture CO_2 + C_{10} (*n*-decane) for temperatures 310.93K, 344.26K and 377.59K (from top to bottom). The description obtained with the SAFT-VR equation of state (continuous curves) is compared with experimental data (filled circles) (Reamer & Sage, 1963).

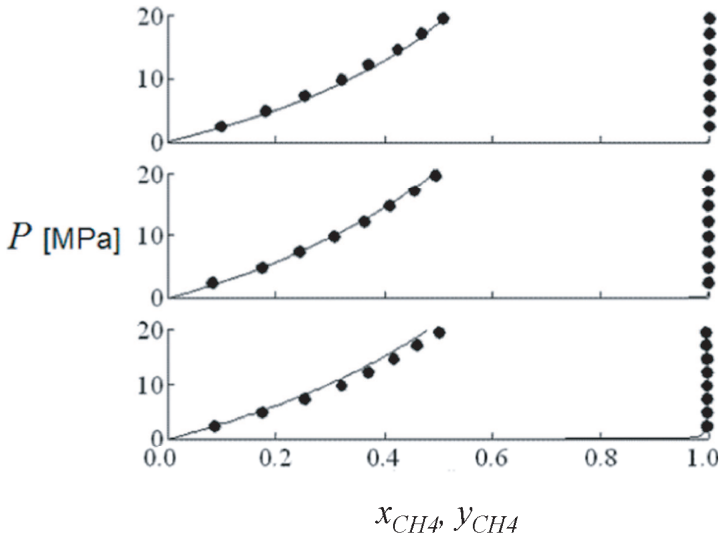

Figure 7: Pressure-composition representation of the vapour-liquid equilibria of the mixture CH_4 + C_{16} (*n*-hexadecane) for temperatures 373.15K, 423.15K and 473.15K (from top to bottom). The predictions obtained with the SAFT-VR equation of state (continuous curves) are compared with experimental data (filled circles) (Sultanov, Skripka & Namiot, 1971)

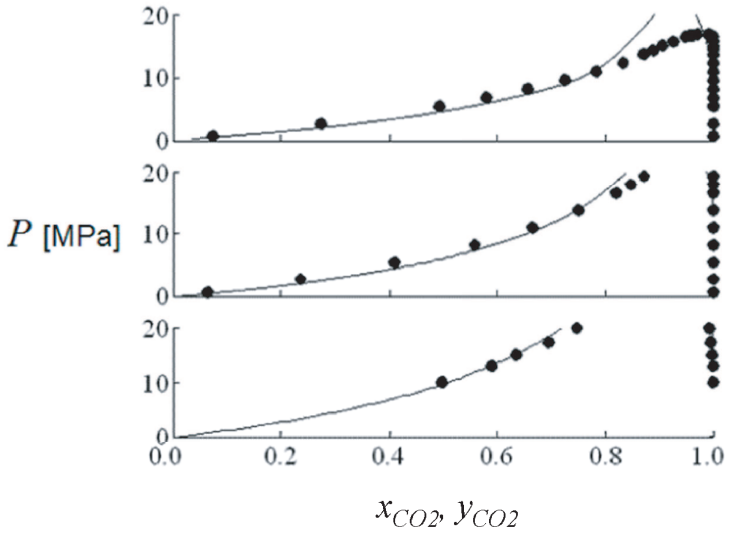

Figure 8: Pressure-composition representation of the vapour-liquid equilibria of the mixture of CO_2 + C_{16} (n-hexadecane) for temperatures 323.15K, 343.15K and 393.20K (from top to bottom). The predictions obtained with the SAFT-VR equation of state (continuous curves) are compared with experimental data (Charoensombut-Amon, Martin & Kobayashi, 1986) for T = 323.15K and 343.15K; (Spee & Schneider, 1991) for T = 393.20K)

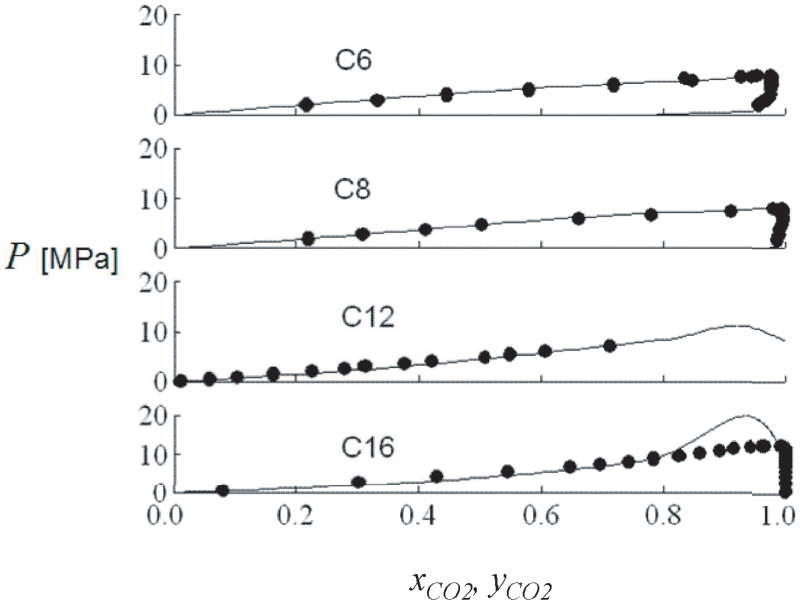

Figure 9: Pressure-composition representation of the vapour-liquid equilibria of the mixture CO_2 + n-alkane for a fixed temperature 313.15K (from top to bottom, n-alkanes are n-hexane C_6, n-octane C_8, n-dodecane C_{12} and n-hexadecane C_{16}). The predictions obtained with the SAFT-VR equation of state (continuous curves) are compared with experimental data (filled circles (Wagner & Wichterle, 1987) for n-hexane; (Chen & Chen, 1992) for n-octane, (Henni, Jaffer & Mather, 1996) for n-dodecane and (Charoensombut-Amon, Martin & Kobayashi, 1986) for n-hexadecane).

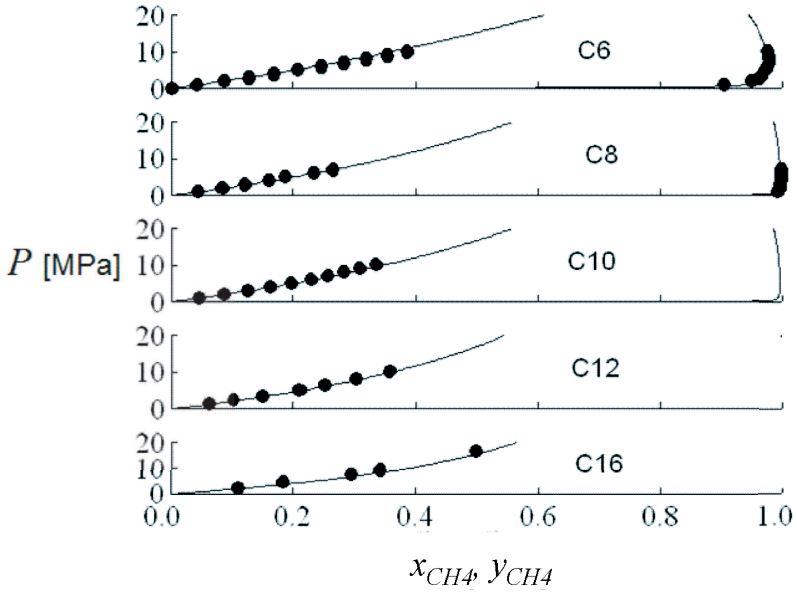

Figure 10: Pressure-composition representation of the vapour-liquid equilibria for the mixture CH_4 + n-alkane for a fixed temperature 323.15K (from top to bottom, n-alkanes are n-hexane C_6, n-octane C_8, n-decane C_{10}, n-dodecane C_{12} and n-hexadecane C_{16} (T=320K for C_{16})). The predictions obtained with the SAFT-VR equation of state (continuous curves) are compared with experimental data (filled circles (Shim & Kohn, 1962) for n-hexane; (Kohn & Bradish, 1964) for n-octane; (Beaudoin & Kohn, 1967) for n-decane; (Srivastan, Darwish, Gasem & Robinson, 1992) for n-dodecane and (M. Glaser, Peters, van der Kool & Lichtenthaler, 1985) for n-hexadecane)

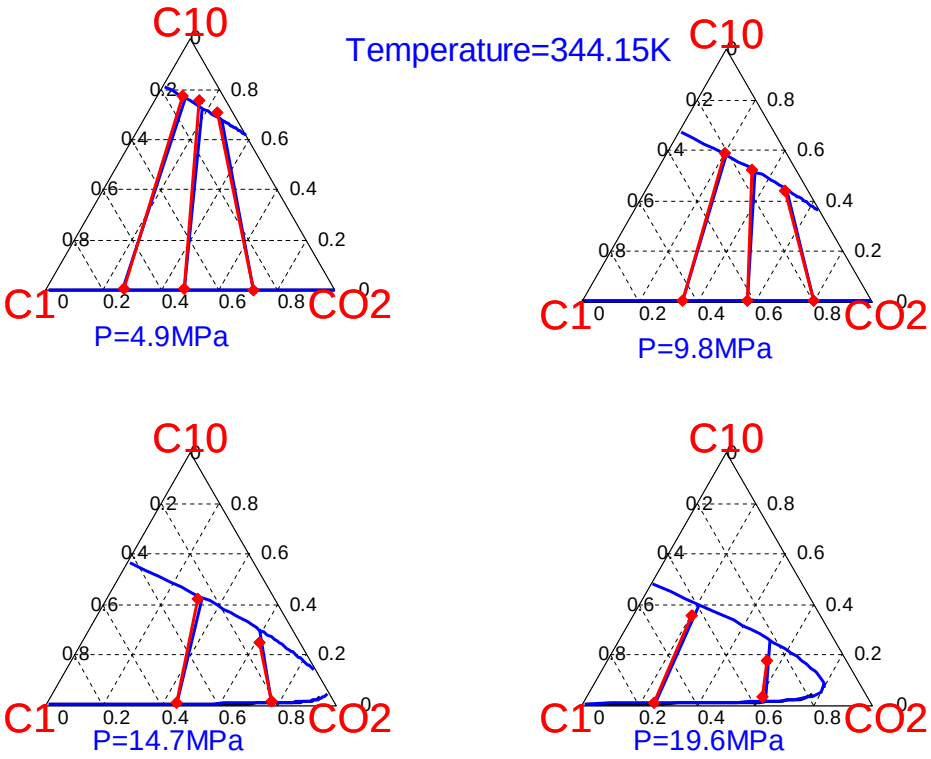

Figure 11: Vapour-liquid equilibrium of the ternary mixture: CO_2 + CH_4 + C_{10} (*n*-decane). Three data sets obtained at different pressures of 4.9 MPa, 9.8 MPa, 14.7 MPa, and 19.6 MPa, and a temperature of 344.15 K, are shown. The experimental points are shown as diamonds (joined by tie lines, (Dunyushkin, Skripka & Nenartovich, 1977)) and the SAFT-VR calculations as the continuous curves.